Chapter 4: Applications of Thermodynamics to the Earth

4.1 INTRODUCTION

In the previous 2 chapters, we developed the fundamental thermodynamic relationships and saw how they are applied to geochemical problems. The tools now in our thermodynamic toolbox are sufficient to deal with many geochemical phenomena. They are not sufficient, however, to deal with all geochemical phenomena. In this chapter, will add a final few thermodynamic tools. These allow us to deal with non-ideal behavior and exsolution phenomena in solids and silicate liquids. With that, we can use thermodynamics to determine the pressure and temperature at which rock assemblages formed, certainly one of the most useful applications of thermodynamics to geology. Along the way, we will see how thermodynamics is related to one of the most useful tools in petrology: phase diagrams. We will then briefly consider how thermodynamics has been used to construct computer models of how magma compositions evolve during melting and crystallization. Finally, we return to the question of non-ideal behavior in electrolyte solutions and examine in more depth the problems of ion association and solvation and how this affects ion activities. Deviations from ideal behavior tend to be greater in solutions of high ionic strength, which includes such geologically important solutions as hydrothermal and ore-forming fluids, saline lake waters, metamorphic fluids, and formation and oil field brines. We briefly examine methods of computing activity coefficients at ionic strengths relevant to such fluids.

4.2 ACTIVITIES IN NON-IDEAL SOLID SOLUTIONS

4.2.1 Mathematical Models of Real Solutions: Margules Equations

Ideal solution models often fail to describe the behavior of real solutions; a good example is water and alcohol, as we saw in Chapter 3. Ideal solutions fail spectacularly when exsolution occurs, such as between oil and vinegar, or between orthoclase and albite, a phenomenon we will discuss in more detail shortly. In non-ideal solutions, even when exsolution does not occur, more complex models are necessary.

Power, or Maclaurin, series are often a convenient means of expressing complex mathematical functions, particularly if the true form of the function is not known, as is often the case. This approach is the basis of Margules† equations, a common method of calculating excess state functions. For example, we could express the excess volume as a power series:

$$\bar{V}_{ex} = A + BX_2 + CX_2^2 + DX_2^3 + \ldots \qquad 4.01$$

where X_2 is the mole fraction of component 2.

Following the work of Thompson (1967), Margules equations are used extensively in geochemistry and mineralogy as models for the behavior of non-ideal solid solutions. It should be emphasized that this approach is completely empirical — true thermodynamic functions are not generally power series. The approach is successful, however, because nearly any function can be *approximated* as a power series. Thus Margules equations are attempts to approximate thermodynamic properties from empirical observations when the true mathematical representation is not known. We will consider two variants of them: the symmetric and asymmetric solution models.

4.2.1.1 The Symmetric Solution Model

In some solutions, a sufficient approximation of thermodynamic functions can often be obtained by using only a second order power series, i.e., in equ. 4.1, $D = E = ... = 0$. Now in a binary solution, the ex-

† Named for Max Margules (1856-1920), an Austrian meteorologist, who first used this approach in 1895.

cess of any thermodynamic function should be entirely a function of mole fraction X_2 (or X_1, however we wish to express it). Put another way, where $X_2 = 0$, we expect $\overline{V}_{ex} = 0$. From this we can see that the first term in Equ. 4.01, A, must also be 0. Thus equation 4.01 simplifies to:

$$\overline{V}_{ex} = BX_2 + CX_2^2 \qquad 4.02$$

The simplest solution of this type would be one that is symmetric about the midpoint, $X_2 = 0.5$; this is called a *Symmetric Solution*. In essence, symmetry requires that:

$$BX_2 + CX_2^2 = BX_1 + CX_1^2 \qquad 4.03$$

Substituting $(1 - X_2)$ for X_1 and expanding the right hand side of 4.3, we have:

$$BX_2 + CX_2^2 = B - BX_2 + C - 2CX_2 + CX_2^2 \qquad 4.04$$

Collecting terms and rearranging:

$$B(2X_2 - 1) = C(1 - 2X_2) \qquad 4.05$$

which reduces to $B = -C$. Letting $W_V = B$ in equation 4.2, we have:

$$\overline{V}_{ex} = W_V X_2 - W_V X_2^2 = W_V X_2 (1 - X_2) = X_1 X_2 W_V \qquad 4.06$$

W is known as an *interaction parameter* because non-ideal behavior arises from *interactions* between molecules or atoms and depends on temperature, pressure, and the nature of the solution, but not on X. Expressions similar to 4.02–4.06 may be written for enthalpy, entropy, and free energy; for example:

$$\overline{G}_{ex} = X_1 X_2 W_G \qquad 4.07$$

The W_G term may be expressed as: $W_G = W_U + PW_V - TW_S$ 4.08

Since the W_H term can be written as: $W_H = W_U + PW_V$

then 4.8 may also be written: $W_G = W_H - TW_S$ 4.08a

The temperature and pressure dependence of W_G are then

$$\left(\frac{\partial W_G}{\partial T}\right)_P = -W_s \qquad 4.09 \qquad \left(\frac{\partial W_G}{\partial P}\right)_T = W_V \qquad 4.10$$

Regular solutions‡ are a special case of symmetric solutions where:

$$W_s = 0 \qquad \text{and therefore} \qquad W_G = W_H$$

Regular solutions correspond to the case where $\Delta S_{ex} = 0$, i.e., where $\Delta S_{mixing} = \Delta S_{ideal}$, and therefore where $W_S = 0$. From equation 4.9, we see that W_G is independent of temperature for regular solutions. Examples of such solutions include electrolytes with a single, uncoupled, anionic or cationic substitution, e.g., $CaCl_2$—$CaBr_2$, or solid solutions where there is a single substitution in just one site (e.g., Mg_2SiO_4—Fe_2SiO_4).

Setting equation 4.7 equal to equation 3.57, we have for binary solutions:

$$\overline{G}_{ex} = X_1 X_2 W_G = RT\left[X_1 \ln \lambda_1 + X_2 \ln \lambda_2\right] \qquad 4.11$$

For a symmetric solution we have the additional constraint that at $X_2 = X_1$, $\lambda_1 = \lambda_2$. From this relationship it follows that:

$$RT \ln \lambda_i = X_j^2 W_G \qquad 4.12$$

This leads to the relationships:

$$\mu_1 = \mu_1^\circ + RT \ln X_1 + X_2^2 W_G \qquad 4.13$$

$$\mu_2 = \mu_2^\circ + RT \ln X_2 + X_1^2 W_G \qquad 4.13a$$

‡ The term regular solution is often used to refer to symmetric solutions. In that case, what we termed a regular solution is called a *strictly regular solution.*

The symmetric solution model should reduce to Raoult's and Henry's Laws in the pure substance and infinitely dilute solution respectively. We see that as $X_1 \rightarrow 1$ equations 4.13 and 4.13a reduce respectively to:

$$\mu_2 = \mu_2^\circ + RT \ln X_2 + W_G \quad 4.15$$

Equation 4.14 is Raoult's Law; letting:

$$\mu^* = \mu^\circ + W_G$$

or $$W_G = RT \ln h$$

then 4.15 is Henry's Law. Thus the interaction parameter can be related to the parameters of Henry's Law, and activity coefficient. In the Margules representation, a solution that is ideal throughout is simply the special case where $A = B = C = D = \ldots = 0$.

4.2.1.2 The Asymmetric Solution Model

Many real solutions, for example mineral solutions with asymmetric solvi, are not symmetric. This corresponds to the case where D in equation 4.01 is nonzero; i.e., we must carry the expansion to the third order. It can be shown that in this case the excess free energy in binary solutions is given by:

$$\overline{G}_{ex} = (W_{G_1} X_2 + W_{G_2} X_1) X_1 X_2 \quad 4.16$$

(You can satisfy yourself that this may be written as a power-series to the third order of either X_1 or X_2.) The two coefficients are related to the Henry's Law constants:

$$W_{G_i} = \mu_i^* - \mu_i^\circ = RT \ln h_i \quad 4.17$$

Activity coefficients are given by:

$$\nu RT \ln \lambda_i = (2W_{G_j} - W_{G_i}) X_j^2 + 2(W_{G_i} - W_{G_j}) X_j^3 \quad 4.18$$

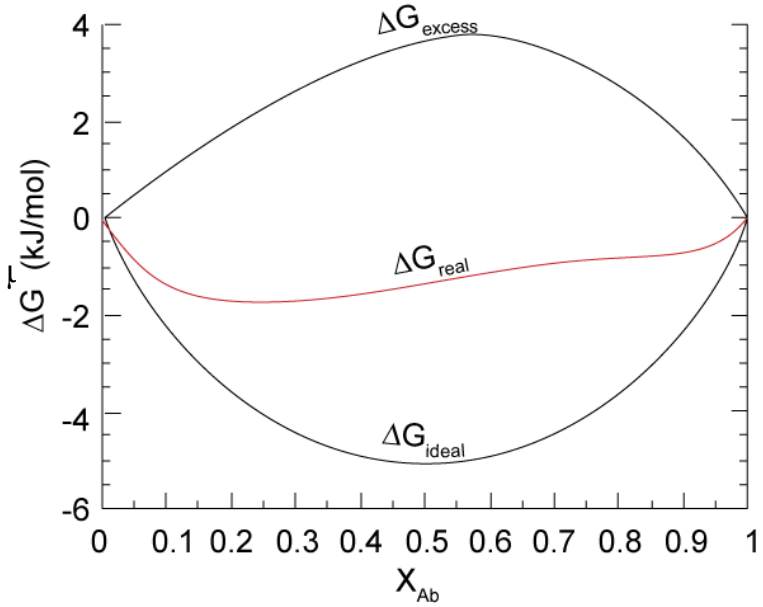

Figure 4.01. Alkali feldspar solid solution computed at 600° C and 200 MPa (2 kb) using the data of Thompson and Waldbaum (1969). $\Delta G_{real} = \Delta G_{ideal} + \Delta G_{excess}$.

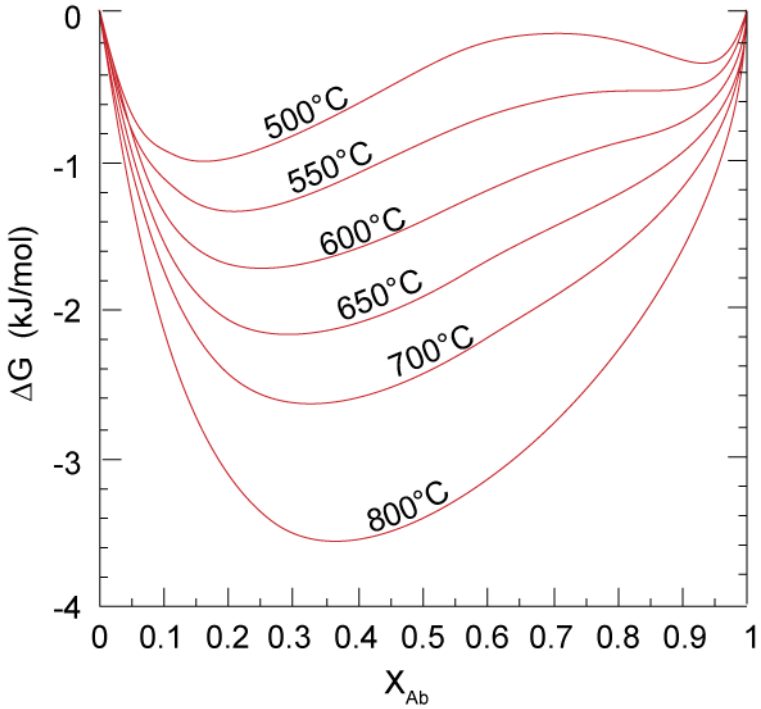

Figure 4.02. ΔG_{real} of alkali feldspar solution computed for a series of temperatures and 200 MPa.

where j=2 when i =1 and visa versa and ν is the stoichiometric coefficient. As for the symmetric solution model, the interaction parameters of the asymmetric model can be expressed as the sum of the W_U, W_V, and W_S interaction parameters to account for temperature and pressure dependencies.

Chapter 4: Applications of Thermodynamics

The alkali feldspars ($NaAlSi_3O_8$ – $KAlSi_3O_8$) are an example of a solid solution exhibiting asymmetric exsolution. Figure 4.01 shows the ΔG_{real}, ΔG_{ideal}, and ΔG_{excess} for the alkali feldspar solid solution computed for 600° C and 200 MPa using the asymmetric solution model of Thompson and Waldbaum (1969). ΔG_{excess} is computed from equation 4.16, ΔG_{ideal} is computed from equation 3.30. Figure 4.02 shows ΔG_{real} for a series of temperatures. Perhaps a clearer picture of how ΔG will vary as a function of both composition and temperature can be obtained by plotting all 3 variables simultaneously, as in Figure 4.03.

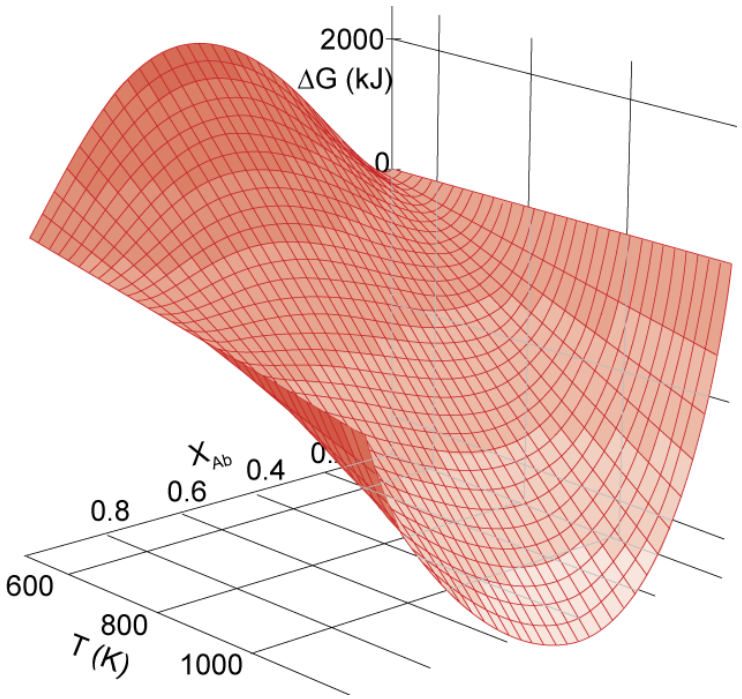

Figure 4.03. ΔG surface for the alkali-feldspar solid solution as a function of the mole fraction albite and temperature.

4.3 Exsolution Phenomena

Now consider a binary system, such as $NaAlSi_3O_8$— $KAlSi_3O_8$ in the example above, of components 1 and 2, each of which can form a pure phase, but also together form a solution phase, which we will call *c*. The condition for spontaneous exsolution of components 1 and 2 to form two phases *a* and *b* is simply that $G_a + G_b < G_c$.

Example 4.1: Computing Activities Using Margules Parameters

Compute the activity of albite in an albite (Ab) and orthoclase (Or) solid solution (alkali feldspar) as a function of the mole fraction of albite from $X_{Ab} = 0$ to 1 at 600° C and 200 MPa. Use the asymmetric solution model and the data of Thompson and Waldbaum (1969) given below.

Alkali Feldspar Margules Parameters

	Ab	Or
W_V (J/MPa-mol)	3.89	4.688
W_S (J/mol)	19.38	16.157
W_H (kJ/mol)	26.485	32.105

Answer: Our first step is to calculate W_G for each end member where $W_G = W_H + W_vP - W_ST$. Doing so, we find W_{GAb} = 10.344 kJ and W_{GOr} = 18.938 kJ. We can then calculate the activity coefficient as a function of X_{Ab} and X_{Or} from equ. 4.19. The activity is then computed from $a = \lambda X_{Ab}$. The results are plotted in Figure 4.4.

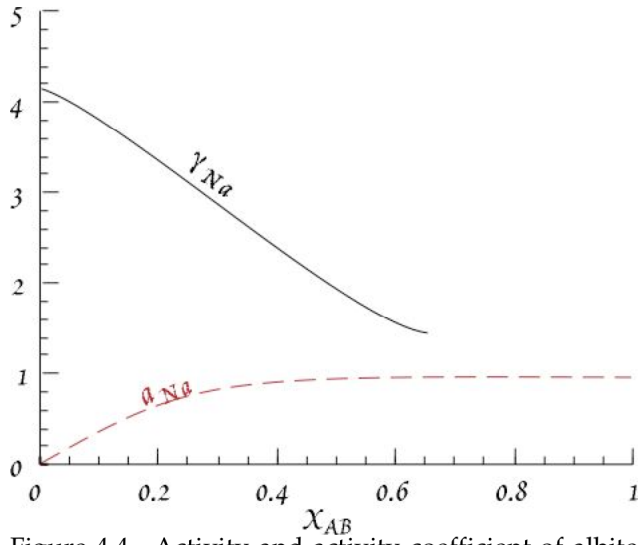

Figure 4.4. Activity and activity coefficient of albite in alkali feldspar solid solution computed at 600° C and 200 MPa using the asymmetric solution model of Thompson and Waldbaum (1969).

CHAPTER 4: APPLICATIONS OF THERMODYNAMICS

As we saw in Chapter 3, the free energy of a real solution can be expressed as the sum of an ideal solution a non-ideal or excess free energy term:

$$G_{real} = G_{ideal} + G_{ex}$$

The free energy of the ideal part is given by:

$$\overline{G}_{ideal} = \sum_i X_i \mu_i^o + RT \sum_i X_i \ln X_1 \qquad (3.31)$$

Further, the ideal part itself consists of two terms, the first term in 3.31 corresponding to the free energy of a mechanical mixture ($G_{mixture}$), the second part being the free energy of ideal mixing ($\Delta G_{ideal\ mixing}$). Figure 4.05a illustrates the variation of G_{excess}, $G_{mixture}$, and G_{ideal} in this hypothetical system. $G_{mixture}$ is simply the free energy of a mechanical mixture of pure components *1* and *2* (e.g., orthoclase and albite). Figure 4.05b illustrates the variation of G_{real} in this system So long as G_{real} is less than $G_{mixture}$, a solution is stable relative to pure phases *1* and *2*. You can see that G_{ideal} is always less than $G_{mixture}$, so as long as the G_{ex} term is not too great. In the hypothetical case illustrated in Fig. 4.05, a solution is always stable relative to a mechanical mixture of the pure end member phases. However, if we look carefully at Fig. 4.05b, we see there is yet another possibility, namely that two phases *a* and *b*, each of which is a *limited* solid solution of components 1 and 2, are stable relative to a single solid solution. Thus at equilibrium, two phases will exsolve from the single solution; this is just what occurs at lower temperatures in the alkali feldspar system. It would be useful if thermodynamics could predict when such exsolution will occur. Let's see if our thermodynamics tools are up to the task.

Looking at Figure 4.02, we see that at 800° C, ΔG_{real} defines a continuously concave upward path, while at lower temperatures, such as 600° C (Figure 4.01), inflections occur and there is a region where ΔG_{real} is concave downward. All this suggests we can use calculus to predict exsolution. For a binary solution of components 1 and 2, the $G_{mixture}$, and $\Delta G_{ideal\ mixing}$ terms are:

$$G_{mixture} = X_1 \mu_1^o + X_2 \mu_2^o$$

$$\Delta G_{ideal\ mixing} = RT(X_1 \ln X_1 + X_2 \ln X_2)$$

Equation 3.31 can thus be written as:

$$\overline{G} = X_1 \mu_1^o + X_2 \mu_2^o + RT(X_1 \ln X_1 + X_2 \ln X_2) + G_{ex} \qquad 4.19$$

Differentiating with respect to X_2 (and recalling that $X_1 = 1 - X_2$), we obtain:

$$\left(\frac{\partial \overline{G}}{\partial X_2}\right) = \mu_2^o - \mu_1^o + RT \ln \frac{X_2}{X_1} + \left(\frac{\partial \overline{G}_{ex}}{\partial X_2}\right) \qquad 4.20$$

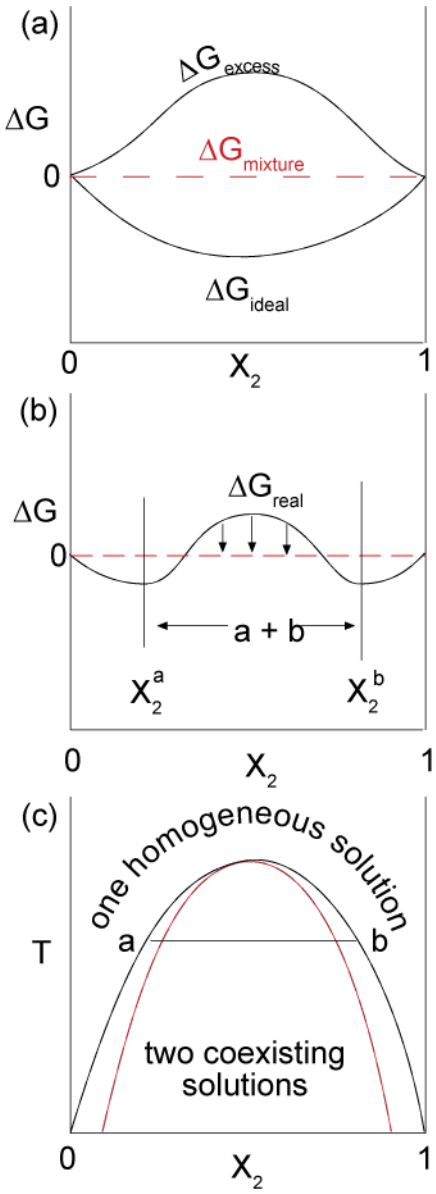

Figure 4.05. (a) Schematic isothermal, isobaric G-X plot for a real solution showing ΔG of mechanical mixing, ideal mixing and excess mixing. (b) Sum of ideal and excess mixing free energies shown in (a). Tangents to the minima give the chemical potentials in immiscible phases *a* and *b*. (c). T-X plot for same system as in (b). Solid line is the *solvus*, dashed line is the *spinodal*. Exsolution may not occur between the spinodal and solvus because the free energy can locally increase during exsolution. After Nordstrom and Munoz (1986).

This is the equation for the slope of the curve of G vs. X_2. The second derivative is:

$$\left(\frac{\partial^2 \overline{G}}{\partial X_2^2}\right) = \frac{RT}{X_1 X_2} + \left(\frac{\partial^2 \overline{G}_{ex}}{\partial X_2^2}\right) \qquad 4.21$$

This tells us how the slope of the curve changes with composition. For an ideal solution, G_{excess} is 0, the second derivative is always positive, and the free energy curve is concave upward. But for real solutions G_{excess} can be positive or negative. If for some combination of T and X (and P), the second derivative of G_{excess} becomes negative and its absolute value is greater than the RT/X_1X_2 term, inflection points appear in the G-X curve. Thus exsolution is thermodynamically favored if for some composition:

$$\frac{RT}{X_1 X_2} + \left(\frac{\partial^2 \overline{G}_{ex}}{\partial X_2^2}\right) \leq 0$$

The inflection points occur where the second derivative is 0, however, as may be seen in Fig. 4.5b, the inflection points do not correspond with the thermodynamic limits of solubility, which in this diagram are between X_2^a and X_2^b.

We can draw a straight line that is tangent to the free energy curve at X_2^a and X_2^b. This line is the free energy of a mechanical mixture of the two limited solutions *a* and *b*. Phase *a* is mostly component 1, but contains X_2^a of component 2. Similarly, phase *b* is mostly component 2 but contains $1 - X_2^b$ of component 1. The mechanical mixture of *a* and *b* has less free energy than a single solution phase everywhere between X_2^a and X_2^b. It is therefore thermodynamically more stable, so exsolution can occur in this region.

In Figure 4.02, we can see inflection points developing at about 650° C in the alkali feldspar solution. The inflection points become more marked and occur at increasingly different values of X_{Ab} as temperature decreases. The alkali feldspar system illustrates a common situation where there is complete solid solution at higher temperature, but decreasing *miscibility* at lower temperature. This occurs because free energy of ideal mixing becomes less negative with decreasing temperature (Figure 3.06).

Figure 4.05c shows a schematic drawing of a temperature–composition plot in which there is complete solution at higher temperature with a widening two-phase region at lower temperatures. The boundary between the two-phase and one-phase regions is shown as a solid line and is known as the *solvus*.

The analysis of exsolution above is relevant to immiscible liquids (e.g., oil and vinegar, silicate and sulfide melts) as well as solids. There is a difference, however. In solids, exsolution must occur through diffusion of atoms through crystal lattices, while in liquids both diffusion and advection serve to redistribute components in the exsolving phases. As exsolution begins, the exsolving phases begin with the

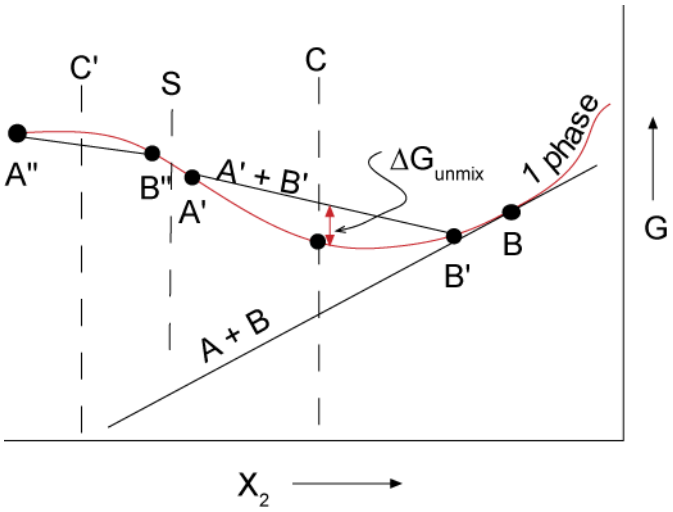

Figure 4.06. A small portion of a *G-X* plot illustrating the origin of the spinodal. The process of exsolution of two phases from a single solid solution must overcome an energy barrier. As exsolution from a solution of composition C begins, the two exsolving phases have compositions that move away from C, e.g., A′ and B′. But the free energy of a mechanical mixture of A′ and B′ has greater free energy, by ΔG_{unmix} than the original single solution phase. Exsolution will therefore be inhibited in this region. This problem does not occur if the original solution has composition C′.

composition of the single solution and must rid themselves of unwanted components. In a solid, this only occurs through diffusion, which is very slow. This leads to a kinetic barrier that often prevents exsolution even though 2 exsolved phases are more stable than 1 solution. This is illustrated in Figure 4.6. For example, consider a solution of composition C. It begins to exsolve protophases of A and B, which initially have compositions A´ and B´. Even though a mechanical mixture of A and B will have lower free energy than solution phase C, A´ and B´, the initial products of exsolution, have higher free energy than C. Furthermore, as exsolution proceeds and these phases move toward compositions A and B, this free energy excess becomes larger. Thus exsolution causes a local increase in free energy and therefore cannot occur. This problem is not encountered at composition C' though, because a mixture of the exsolving protophases A" and B" has lower free energy than original solution at C´. Thus the actual limit for exsolution is not tangent points such as B but at inflection points (where $\partial^2 G/\partial X^2 = 0$) such as S. The locus of such points is plotted in Figure 4.05c as the dashed red line and is known as the *spinodal*.

4.4 THERMODYNAMICS AND PHASE DIAGRAMS

A *phase diagram* is a representation of the regions of stability of one or more phases as a function of two or more thermodynamic variables such as temperature, pressure, or composition. In other words, if we plot 2 thermodynamic variables such as temperature and pressure or temperature and composition, we can define an area on this plot where a phase of interest is thermodynamically stable. Figure 4.07 is an example of a T-P phase diagram for a 1-component system: SiO_2. The diagram shows the SiO_2 phase stable for a given combination of pressure and temperature. Figure 4.08 is an example of a simple T-X diagram for the two-component system diopside-anorthite ($CaMgSi_2O_6$ or clinopyroxene and Ca-plagioclase, $CaAl_2Si_2O_8$; two of the more common igneous rock forming minerals). In multicomponent systems we must always be concerned with at least 3 thermodynamic variables: P, T, and X. Thus any T-X phase diagram will be valid for only one pressure, 0.1 MPa (1 bar ≈ 1 atm) in this case. Of course, with a three dimensional drawing it is possible to represent both temperature and pressure as well as composition in a binary system.

It should not surprise you at this point to hear that the phase relationships in a chemical system are a function of the thermodynamic properties of that system. Thus phase diagrams, such as Figures 4.07 and 4.08, can be constructed from thermodynamic data. Conversely, thermodynamic information can be deduced from phase diagrams.

Let's now see how we can construct phase diagrams, specifically T-X diagrams, from thermodynamic data. Our most important tool in doing so will be the $\bar{G}$ – X diagrams that we have already encountered. *The guiding rule in constructing phase diagrams from $\bar{G}$ – X diagrams is that the stable phases are those that combine to give the lowest $\bar{G}$.* Since a $\bar{G}$ – X diagram is valid for only one particular temperature, we will need a number of $\bar{G}$ – X diagrams at different temperatures to construct a single T – X diagram (we could also construct P – X diagrams from a number of $\bar{G}$ – X diagrams at different pressures). Before we begin, we will briefly consider the thermodynamics of melting in simple sys-

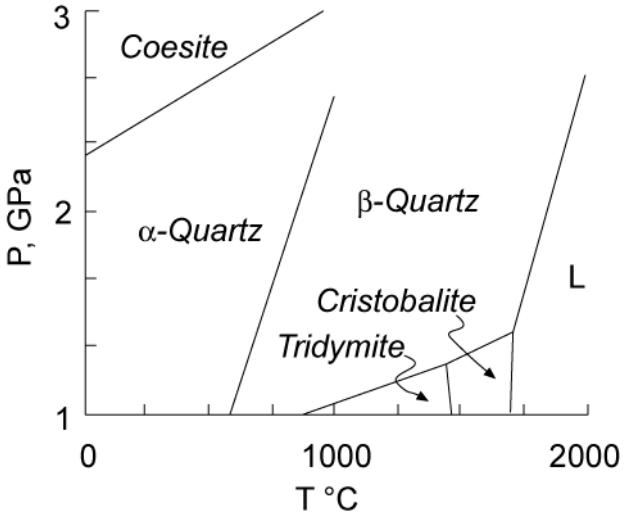

Figure 4.07. P-T phase diagram for SiO_2. This system has 1 component but 7 phases. L designates liquid, dashed lines indicate where phase boundaries are uncertain. The α—β quartz transition is thought to be partially second order, that is, it involves only stretching and rotation of bonds rather than a complete reformation of bonds as occurs in first order phase transitions.

tems.

4.4.1 The Thermodynamics of Melting

One of the more common uses of phase diagrams is the illustration of melting relationships in igneous petrology. Let's consider how our thermodynamic tools can be applied to understanding melting relationships. We begin with melting in a simple one-component system, for example quartz. At the melting point, this system will consist of two phases: a solid and a melt. At the melting point, the liquid and solid are in chemical equilibrium. Therefore, according to equation 3.17: $\mu_l = \mu_s$.

The Gibbs Free Energy of melting, ΔG_m, must be 0 at the melting point (and only at the melting point). Since

$$\Delta G_m = \Delta H_m - T_m \Delta S_m \qquad 4.22$$

and $\Delta G_m = 0$ at T_m, then:

$$\Delta H_m = T_m \Delta S_m$$

where ΔH_m is the heat (enthalpy) of melting or fusion*, T_m is the melting temperature, and ΔS_m is the entropy change of melting. Thus the melting temperature of a pure substance is simply:

$$\boxed{T_m = \frac{\Delta H_m}{\Delta S_m}} \qquad 4.23$$

This is a very simple, but very important, relationship. This equation tells us that temperature of melting of a substance is the ratio of the enthaply change to entropy change of melting. Also, if we can measure temperature and enthalpy change of the melting reaction, we can calculate the entropy change.

The pressure dependence of the melting point is given by the Clapeyron Equation:

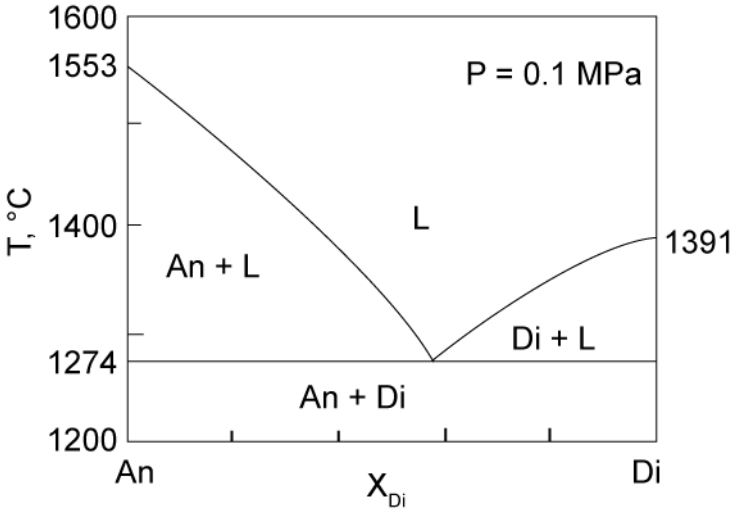

Figure 4.08. Phase diagram (T-X) for the two-component system diopside-anorthite at 1 atm. Four combinations of phases are possible as equilibrium assemblages: liquid (L), liquid plus diopside (L + Di), liquid plus anorthite (L + An), and diopside plus anorthite.

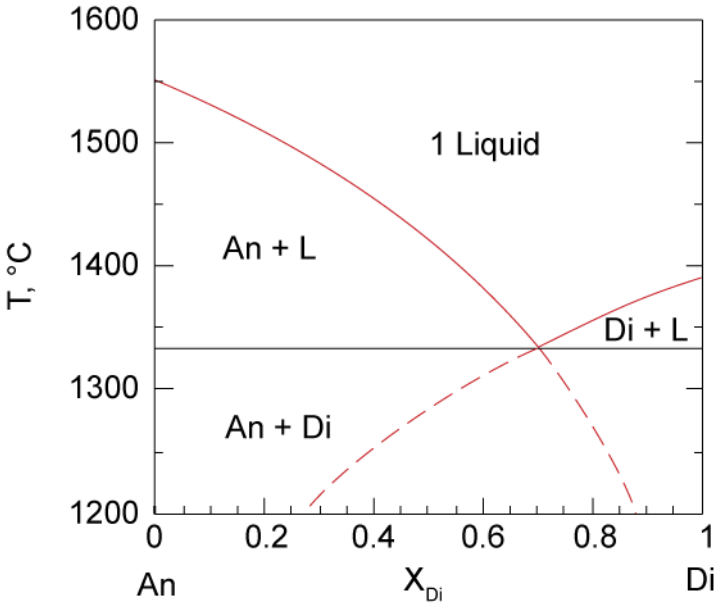

Figure 4.09. Computed phase diagram for the system Anorthite-Diopside ($CaAl_2Si_2O_8$–$CaMgSi_2O_6$). The eutectic occurs at X_{Di} = 0.7 and 1334°C. The dashed lines beyond the eutectic give the apparent melting points of the components in the mixture.

* The heat of fusion is often designated by ΔH_f. I have chosen to use the subscript *m* to avoid confusion with heat of formation, for which we have already been using the subscript *f*.

$$\frac{dT}{dP} = \frac{\Delta V_m}{\Delta S_m} \qquad 4.24$$

Precisely similar relationships hold for vaporization (boiling). Indeed, the temperature and pressure boundaries between any two phases, such as quartz and tridymite, calcite and aragonite, etc., depend on thermodynamic properties in an exactly analogous manner.

In equation 3.66 we found that addition of a second component to a pure substance depresses the melting point. Assuming ΔS_m and ΔH_m are independent of temperature, we can express this effect as:

$$\frac{T_{i,m}}{T} = 1 - \frac{R \ln a^{\ell}_{i,m}}{\Delta S_{i,m}} \qquad 4.25$$

Since enthalpies of fusion, rather than entropies, are the quantities measured, equation 4.25 may be more conveniently expressed as:

$$\frac{T_{i,m}}{T} = 1 - \frac{T_{i,m} R \ln a^{\ell}_{i,m}}{\Delta H_{i,m}} \qquad 4.26$$

Example 4.2 shows how the approximate phase diagram for the diopside-anorthite system (Figure 4.09) may be constructed using this equation.

It must be emphasized that in deriving equation 3.66, and hence the equations 4.25 and 4.26, we made the assumption that the solid was a pure phase. This assumption is a reasonably good one for ice, and for anorthite-diopside binary system, but it is not generally valid. Should the solid or solids involved exhibit significant solid solution, this assumption breaks down and these equations are invalid. In that case, melting phase diagrams can still be constructed from thermodynamic equations, but we need to model solid solution as well as the liquid one. Section 4.4.2.1 below illustrates an example (Anorthite-Albite) where the two solutions can be modeled as ideal.

4.4.2 Thermodynamics of Phase Diagrams for Binary Systems

In a one component system, a phase boundary, such as the melting point, is univariant since at that point two phases coexist and f = c- p + 2 = 1 - 2 + 2 = 1. Thus specifying either temperature or pressure fixes the other. A three-phase point, e.g., the triple point of water, is invariant. Hence simply from knowing that three phases of water coexist (i.e., knowing we are at the triple point), we know the temperature and pressure.

In binary systems, the following phase assemblages are possible according to the Gibbs Phase Rule (ignoring for the moment gas phases):

	Phases	Free compositional variables
Univariant	2 solids + liquid, 2 liquids + solid, 3 solids or liquids	0
Divariant	1 solid + 1 liquid, 2 solids, 2 liquids	0
Trivariant	1 solid or 1 liquid	1

When a $\bar{G}$ -X diagram is drawn, it is drawn for a specific temperature and pressure, i.e., $\bar{G}$ -X are isobaric and isothermal. Thus we have already fixed two variables, and the compositions of all phases in univariant and divariant assemblages are fixed by virtue of our having fixed T and P. Only in trivariant systems are we free to choose the composition of a phase on a $\bar{G}$ -X diagram. Figure 4.10 is schematic diagram of a two component, one phase (trivariant) assemblage, in which there is complete solution between component *1* and component *2*. This phase might be either a liquid, or a solid such as plagioclase. The composition of the phase may fall anywhere on the curve. Of course, since this diagram applies only to one temperature, we cannot say from this diagram alone that there will be complete solution at all temperatures.

EXAMPLE 4.2: CALCULATING MELTING CURVES

Using the data given below and assuming (1) that the melt is an ideal solution and (2) diopside and anorthite solids are pure phases, calculate a T-X phase diagram for melting of an anorthite-diopside mixture.

	T_m	ΔH_m
	° C	joules/mole
Diopside	1391	138100
Anorthite	1553	136400

(Data from Stebbins et al., 1983)

Answer: Solving equation 4.26 for T, and replacing activity with mole fraction (since we may assume ideality), we have:

$$T = \frac{\Delta H_{i,m}}{\Delta H_{i,m}/T_{i,m} - R \ln X_i^{\ell}} \qquad 4.27$$

We then calculate T for every value of X_{An} and X_{Di}. This produces two curves on a T-X plot, as shown in Figure 4.09. The curves intersect at the *eutectic*, or lowest point at which melt may exist in the system.

Comparing our result with the actual phase relationships determined experimentally (Figure 4.08), we see that while the computed phase diagram is similar to the actual one, our computed eutectic occurs at $X_{Di} = 0.70$ and 1335° C and the actual eutectic occurs at $X_{Di} \approx 0.56$ and 1274° C. The difference reflects the failure of the several assumptions we made. First, and most importantly, silicate liquids are not ideal solutions. Second, the entropies and enthalpies of fusion tend to decrease somewhat with decreasing temperature, violating the assumption we made in deriving equation 4.26. Third, the diopside crystallizing from anorthite-diopside mixtures is not pure, but contains some Al and an excess of Mg.

Figure 4.11 illustrates four possible divariant systems. The first case (Figure 4.11a) is that of a liquid solution of composition L' in equilibrium with a solid of fixed composition S_2 (pure component 2). Because the system is divariant, there can be only one possible liquid composition since we have implicitly specified P and T. As usual, the equilibrium condition is described by $\mu_i^l = \mu_i^s$ (equation 3.17). For $i = 2$, this means the tangent to the free energy curve for the melt must intersect the $X_2 = 1$ line at μ_2^s as is shown. In other words, the chemical potential of component 2 in the melt must be equal to the chemical potential of component 2 in the solid. Again, this diagram is valid for only one temperature; at any other temperature, the free energy curve for the liquid would be different, but the composition of this new liquid in equilibrium with solid S_2 would still be found by drawing a tangent from S_2 to the free energy curve of the liquid. At sufficiently high temperature, the tangent would always intersect below S_2. The temperature at which this first occurs is the melting temperature of S_2 (because it is the point at which the free energy of a liquid of pure 2 is less than the solid). The shaded region shows the compositions of systems that will have a combination of solid S_2 and liquid L′ as their equilibrium phases as this temperature.

We can also think of the tangent line as defining the free energy of a mechanical mixture of S_2 and L'. In the range of compositions denoted by the shaded region, this mixture has a lower free energy than the liquid solution, hence at equilibrium we expect to find this mixture rather than the liquid solution.

Figure 4.11b illustrates a system with a liquid plus a solid solution, each of which has its own G-X curve. Again, the equilibrium condition is $\mu_i^l = \mu_i^s$ so the compositions of the coexisting liquid and solid are given by a tangent to both

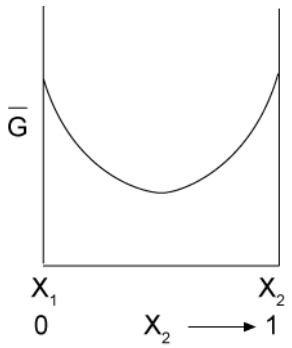

Figure 4.10. Molar free energy vs. composition ($\bar{G} - X_2$) for a one-phase assemblage that exhibits complete solution of either a liquid or solid.

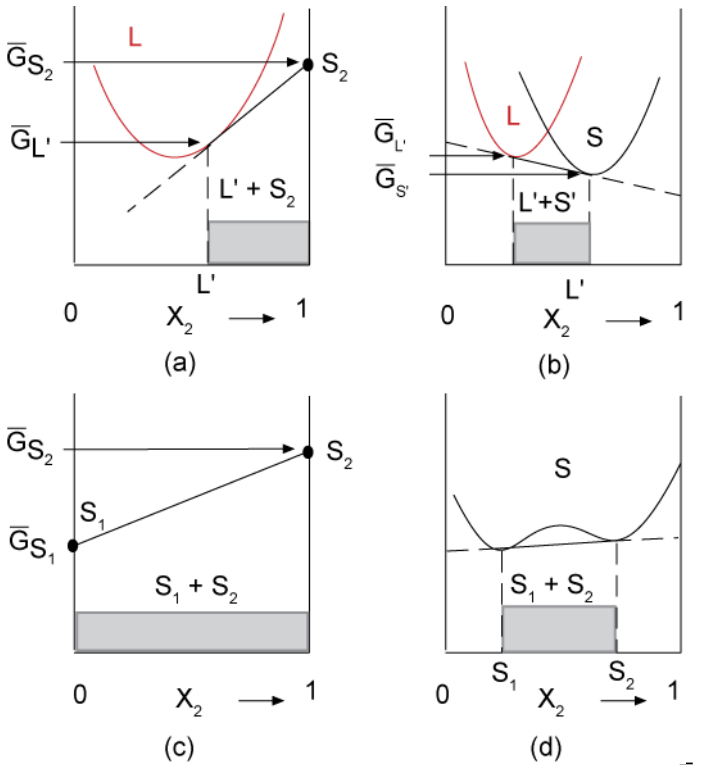

Figure 4.11. Plot of molar free energy vs. composition ($\bar{G}$ – X_2) for two phase divariant systems. (a) shows a liquid solution (*L*) in equilibrium with a solid (S_2) of pure X_2. The shaded area shows the range of composition of systems for which *L'* and S_2. (b) is the case of where both solid and liquid have variable composition. Equilibrium compositions are determined by finding a tangent to both free energy curves. *L'* and *S'* will be the equilibrium phases for systems having compositions in the shaded area. (c) is the case of 2 immiscible solids. (d) shows two limited solid solutions of composition S_1 and S_2. In the case, the compositions of the solids are given by the point where a straight line is tangent to the curve in two places.

curves. Since the system is divariant and we have fixed P and T the compositions of the solutions are fixed. All system compositions in the shaded region can be accommodated by a mixture of liquid and solid. Compositions lying to the left of the region would have only a liquid; compositions to the right of the shaded region would be accommodated by a solid solution.

Figure 4.11c illustrates the case of two immiscible solids (pure components *1* and *2*). The molar free energy of the system is simply that of a mechanical mixture of S_1 and S_2: a straight line drawn between the free energy points of the two phases.

Figure 4.11d illustrates the case of a limited solution. We have chosen to illustrate a solid solution, but the diagram would apply equally well to the case of two liquids of limited solubility.

Figure 4.12a shows the case of two solid solutions plus one liquid. The chemical potential of each component in each phase must be equal to the chemical potential of that component in every other phase, so chemical potentials are given by tangents to all three phases. This is an univariant system, specifying either temperature, pressure, or the composition of a phase fixes other variables in the system. Because of this, if we move to a slightly higher or low temperature at fixed pressure one of the phases must be eliminated in a *phase elimination reaction*. If the liquid is the liquid is between the two solids in composition, the reaction is known as a *eutectic*, which is the lowest temperature at which the liquid can exist. Moving to a higher temperature would result in elimination of one of the solids. If, alternatively, the liquid is not between two solids (for example, if the curves L and S2 in Fig. 4.12 were switched), the reaction would be known as a peritectic, and moving to lower temperature eliminates one of the solids. Thus, it is possible for a liquid to persist below a peritectic if the composition is right, but a liquid will never persist at equilibrium below a euctectic. Figure 4.12b is a eutectic in a system where the two solids are the phases of pure components 1 and 2. A line drawn between the free energies of the pure components is also tangent to the liquid curve.

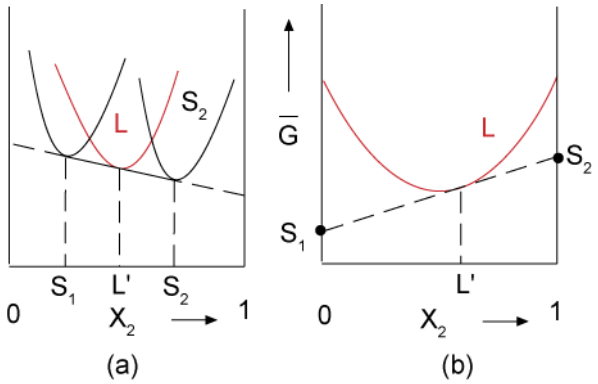

Figure 4.12. Two univariant systems: a liquid plus two solid solutions, and two pure solids and a liquid. Since these systems are univariant, they occur only at one fixed T if P is fixed.

this system. Since both the solid and liquid exhibit complete solution, we need to consider G-X curves for both.

We start at the highest point at which liquid and solid coexist, T_m (T_1) for anorthite. Here the solid and liquid curves both have the same value at X_{An} = 1; i.e., they are at equilibrium. A G-X plot above this temperature would show the curve for the liquid to be everywhere below that of the solid, indicating the liquid to be the stable phase for all compositions.

At a somewhat lower temperature (T_2), we see that the curves for the solid and liquid intersect at some intermediate composition. To the right, the curve for the solid is lower than that of the liquid, and tangents to the solid curve extrapolated to both X_{Ab}=1 and X_{An}=1 are always below the curve for the liquid, indicating the solid is the stable phase. As we move toward *Ab* (left) in composition, tangents to the solid curve eventually touch the curve for the liquid. The point where the tangent touches each curve gives composition of the liquid and the solid stable at this temperature. In the compositional range between the points where the tangent touches the two curves, the tangent is below both curves, thus a mechanical mixture of solid and liquid is stable over this compositional range at this temperature. For compositions to the left of the point where the tangent touches the liquid curve, the liquid curve is lower than both the solid curve and a tangent to both, so it is stable relative to

4.4.2.1 An Example of a Simple Binary System with Complete Solution: Albite–Anorthite

Phase diagrams in T-X space can be constructed by analyzing G-X diagrams at a series of temperatures. Let's examine how this can be done in the case of a relatively simple system of two components albite ($NaAlSi_3O_8$) and anorthite ($CaAl_2Si_2O_8$) whose solid (plagioclase) and liquid exhibit complete solid solution. Figure 4.13 shows G-X diagrams for various temperatures as well as a T-X phase diagram for

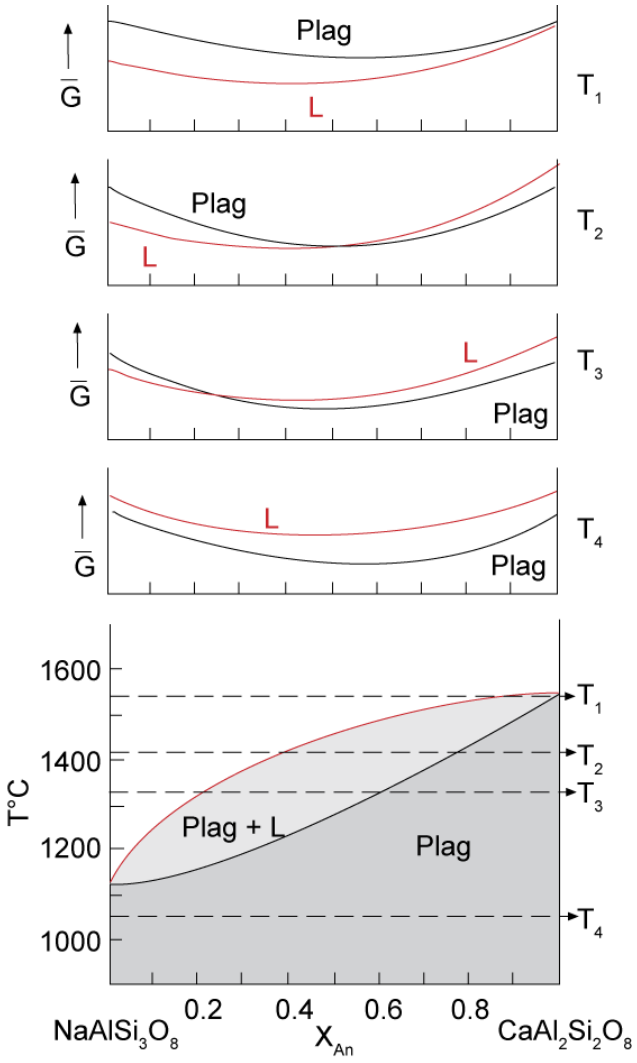

Figure 4.13. G-X diagrams and a T-X phase diagram for the plagioclase-liquid system. After Richardson and McSween (1987).

both the solid and any mixture of solid and liquid.

Going to progressively lower temperatures (e.g., T_3), the points where a tangent intersects the two curves move toward Ab (to the left). Eventually, at a sufficiently low temperature (T_4), the curve for the solid is everywhere below that of the liquid and only solid solution is stable. By extracting information from G-X curves at a number of temperatures, it is possible to reconstruct the phase diagram shown at the bottom of Figure 4.13.

Since both the solid and liquid show complete miscibility in this system, we will make the simplifying assumption that both solutions are ideal and do an approximate mathematical treatment. We recall that the condition for equilibrium was:

$$\mu_i^{\alpha} = \mu_i^{\beta}$$

We can express the chemical potential of each component in each phase as:

$$\mu_i^{\alpha} = \mu_i^{o\alpha} + RT \ln X_i^{\alpha} \qquad 4.28$$

Combining these relationships, we have:

$$\mu_{Ab}^{o\ell} - \mu_{Ab}^{os} = RT \ln\left(\frac{X_{Ab}^{s}}{X_{Ab}^{\ell}}\right) \quad 4.29 \qquad \text{and} \qquad \mu_{An}^{o\ell} - \mu_{An}^{os} = RT \ln\left(\frac{X_{An}^{s}}{X_{An}^{\ell}}\right) \quad 4.30$$

Here our standard states are the pure end members of the melt and solid. The left side of both of these equations corresponds to the standard free energy change of crystallization, thus:

$$\Delta\bar{G}_m^{Ab} = RT \ln\left(\frac{X_{Ab}^{s}}{X_{Ab}^{\ell}}\right) \qquad 4.31 \qquad \text{and} \qquad \Delta\bar{G}_m^{An} = RT \ln\left(\frac{X_{An}^{s}}{X_{An}^{\ell}}\right) \qquad 4.32$$

Both sides of these equations reduce to 0 if and only if $X_i^{\ell} = X_i^{s} = 1$ and $T = T_m$. Rearranging:

$$X_{Ab}^{s} = X_{Ab}^{\ell} e^{-\Delta\bar{G}_m^{Ab}/RT} \qquad 4.33$$

$$X_{An}^{s} = X_{An}^{\ell} e^{-\Delta\bar{G}_m^{An}/RT} \qquad 4.34$$

Thus the fraction of each component in the melt can be predicted from the composition of the solid and thermodynamic properties of the end members. Since $X_{An}^{\ell} = 1 - X_{Ab}^{\ell}$ and $X_{An}^{s} = 1 - X_{Ab}^{s}$, we can combine equations 4.33 and 4.34 to obtain:

$$\left(1 - X_{Ab}^{\ell}\right) e^{-\Delta\bar{G}_m^{An}/RT} = 1 - X_{Ab}^{\ell} e^{-\Delta\bar{G}_m^{Ab}/RT} \qquad 4.35$$

and rearranging yields:

$$X_{Ab}^{\ell} = \frac{1 - e^{-\Delta\bar{G}_m^{An}/RT}}{e^{-\Delta\bar{G}_m^{Ab}/RT} - e^{-\Delta\bar{G}_m^{An}/RT}} \qquad 4.36$$

The point is that *the mole fraction of any component of any phase in this system can be predicted from the thermodynamic properties of the end-members*. We must bear in mind that we have treated this as an ideal system; i.e., we have ignored any G_{excess} term. Nevertheless, the ideal treatment is relatively successful for the plagioclase system. For non-ideal systems, we merely replace mole fraction in the above equations with activity. Provided they are known, interaction parameters can be used to calculate activity coefficients (e.g., equations 4.18 or 4.12 as the case may be). Beyond that, non-ideal systems can be treated in a manner exactly analogous to the treatment above.

4.5 GEOTHERMOMETRY AND GEOBAROMETRY

An important task in geochemistry is estimating the temperature and pressure at which mineral assemblages equilibrate. The importance extends beyond petrology to tectonics and all of geology because it reveals the conditions under which geological processes occur. Here we take a brief look at the thermodynamics underlying geothermometry and geobarometry.

Geothermometry and geobarometry involve two nearly contradictory assumptions. The first is that the mineral assemblage of interest is an equilibrium one, the second is that the system did not re-

equilibrate during the passage through lower P and T conditions that brought the rock to the surface where it could be collected. As we will see in the next chapter, reaction rates depend exponentially on temperature, hence these assumptions are not quite as contradictory as they might seem. In this section, we will focus only on "chemical" thermobarometers. In Chapter 9, we will see that temperatures can also be deduced from the distribution of isotopes between phases.

4.5.1 Theoretical considerations

In general, geobarometers and geothermometers make use of the pressure and temperature dependence of the equilibrium constant, K. In Section 3.9 we found that $\Delta G^\circ = -RT \ln K$. Assuming that ΔC_p and ΔV of the reaction are independent of temperature and pressure, we can write:

$$\Delta G^o = \Delta H^o_{T,P_{ref}} - T\Delta S^o_{T,P_{ref}} + \Delta V^o_{T,P_{ref}}(P - P_{ref}) = -RT \ln K \qquad 4.37$$

where the standard state of all components is taken as the pure phase at the temperature and pressure of interest, and the enthalpy, entropy and volume changes are for the temperature of interest and a reference pressure (generally 0.1 MPa).

Solving 4.37 for ln K and differentiating the resulting equation with respect to temperature and pressure leads to the following relations:

$$\left(\frac{\partial \ln K}{\partial T}\right)_P = \frac{\Delta H^o_{T,P_{ref}} + \Delta V^o_{T,P_{ref}}(P - P_{ref})}{RT^2} \qquad 4.38$$

and

$$\left(\frac{\partial \ln K}{\partial P}\right)_T = \frac{\Delta V^o_{T,P_{ref}}}{RT} \qquad 4.39$$

These equations provide us with the criteria for reactions that will make good geothermometers and geobarometers. For a good geothermometer, we want the equilibrium constant to depend heavily on T, but be approximately independent of P. Looking at equation 4.38, we see this means the ΔH term should be as large as possible and the ΔV term as small as possible. A fair amount of effort was devoted to development of a geothermometer based on the exchange of Fe and Mg between olivine and pyroxenes in the late 1960's. The effort was abandoned when it was shown that the ΔH for this reaction was very small. As a rule, a reaction should have a ΔH° of at least 1 kJ to be a useful geothermometer. For a good geobarometer, we want the ΔV term to be as large as possible. Even though the rhodonite ($[Mn,Fe,Ca]SiO_3$) and pyroxmangite ($[Mn,Fe]SiO_3$) pairs commonly occur in metamorphic rocks, the reaction rhodonite → pyroxmangite does not make a useful geobarometer because the ΔV of reaction is only 0.2 cc/mol. In general, a reaction should have a ΔV of greater than 2 cc/mol if it is to be used for geobarometry.

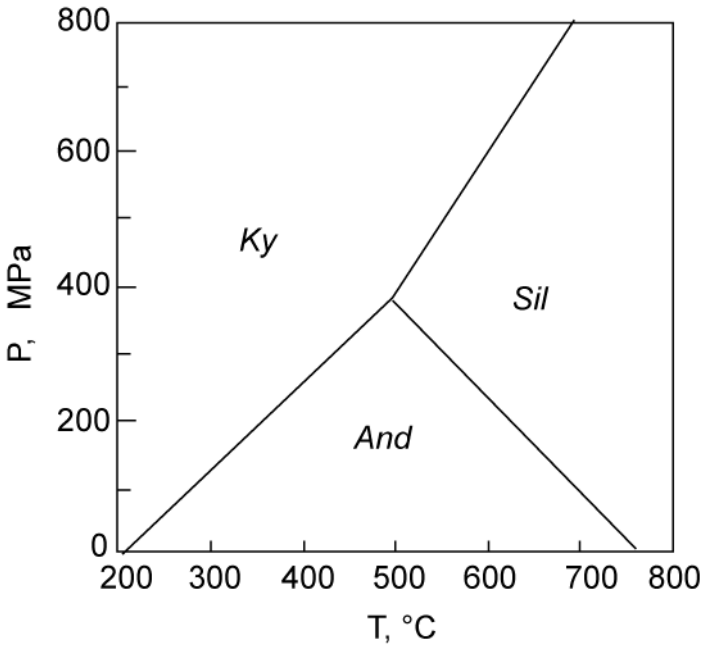

Figure 4.14. Phase diagram for Al_2SiO_5 (kyanite-sillimanite-andalusite) as determined by Holdaway (1971).

The following discussion presents a few examples of useful chemical geothermometers and geobarometers (since

most reactions are both temperature and pressure dependent, it is perhaps more accurate to use the term "thermobarometer"). It is not an exhaustive treatment, nor should it be inferred that those examples discussed are in any way superior to other geothermometers and geobarometers. Reviews by Essene (1982, 1989), Bohlen and Lindsley (1987), and Powell and Holland (2008) summarize a wide range of igneous and metamorphic thermobarometers.

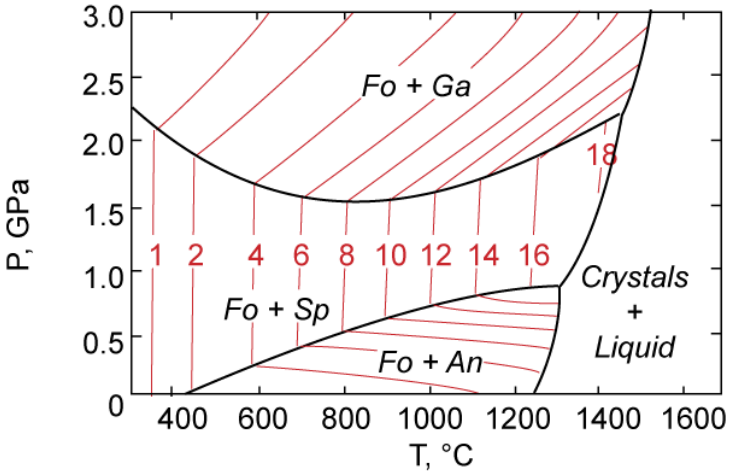

Figure 4.15. Isopleths of Al in orthopyroxene (thin red lines; weight percent) coexisting with forsterite plus and aluminous phase in the CMAS (Ca-Mg-Al-Si) system. After Gasparik (1984).

4.5.2 Practical Thermobarometers

4.5.2.1 Univariant Reactions and Displaced Equilibria

We can broadly distinguish 3 main types of thermobarometers. The first is the *univariant reaction*, in which the phases have fixed compositions. They are by far the simplest, and often make good geobarometers as the ΔV of such reactions is often large. Examples include the graphite-diamond transition, any of the SiO_2 transitions (Figure 4.07), and the transformations of Al_2SiO_5, shown in Figure 4.14. While such thermobarometers are simple, their utility for estimating temperature and pressure is limited. This is because exact temperatures and pressures can be obtained only if two or more phases coexist, for example, kyanite and andalusite in Figure 4.14. If kyanite and andalusite are both found in a rock, we can determine either temperature or pressure if we can independently determine the other. Where 3 phases, kyanite, sillimanite, and andalusite coexist the system is invariant and P and T are fixed. If only one phase occurs, for example sillimanite, we can only set a range of values for temperature and pressure. Unfortunately, the latter case, where only 1 phase is present, is the most likely situation. It is extremely rare that kyanite, sillimanite, and andalusite occur together.

The term *displaced equilibria* refers to variations in the temperature and pressure of a reaction that results from appreciable solution in one or more phases. Thermobarometers based on this phenomenon are more useful than univariant reactions because the assemblage can coexist over a wide range of P and T conditions. In the example shown in Figure 4.15, the boundaries between garnet-bearing, spinel-bearing, and plagioclase-bearing assemblages are curved, or "displaced" as a result of the solubility of Al in enstatite. In addition to the experimental calibration, determination of P and T from displaced equilibria requires (1) careful determination of phase composition and (2) an accurate solution model.

Geobarometers based on the solubility of Al in pyroxenes have been the subject of extensive experimental investigations for the past 25 years. The general principal is illustrated in Figure 4.15, which shows the concentration of Al in orthopyroxene (opx) coexisting with olivine (forsterite) and an aluminous phase, anorthite, spinel, or garnet. The Al content of opx depends almost exclusively on pressure in the presence of anorthite, is essentially independent of pressure in the presence of spinel, and depends on both temperature and pressure in the presence of garnet. Orthopyroxene-garnet equilibrium has proved to be a particularly useful geobarometer.

Garnet is an extremely dense phase. So we might guess that the ΔV of reactions that form it will be comparatively large, and therefore that it is potentially a good geobarometer. The concentration of Al in opx in equilibrium with garnet may be used as a geobarometer if temperature can be independently determined. Although there has been a good deal of subsequent work and refinement of this

geobarometer, the underlying thermodynamic principles are perhaps best illustrated by considering the original work of Wood and Banno (1973).

Wood and Banno (1973) considered the following reaction:

$$Mg_2Si_2O_6 + MgAl_2SiO_6 \rightleftarrows Mg_3Al_2Si_3O_{12} \qquad 4.40$$

Opx Solid Solution $\rightleftarrows$ Pyrope Garnet

In developing a geobarometer based on this reaction, they had to overcome a number of problems. First, the substitution of Al in orthopyroxene is a coupled substitution. For each atom of Al substituting in the M1 octahedral site, there must be another Al atom substituting for SiO_2 in the tetrahedral site. Second, there was a total lack of thermodynamic data on the $MgAl_2SiO_6$ phase component. Data was lacking for a good reason: the phase does not exist and cannot be synthesized as a pure phase. Another problem was the apparent non-ideal behavior of the system, which was indicated by orthopyroxenes in Fe- and Ca-bearing systems containing less alumina than in pure MgO systems at the same pressure.

The equilibrium constant for reaction 4.40 is:

$$K = \frac{a_{Mg_3Al_2Si_3O_{12}}}{a_{Mg_2Si_2O_6}\, a_{MgAl_2SiO_6}} \qquad 4.41$$

where the activities in the denominator represent the activities of the enstatite and the hypothetical aluminous enstatite phase components in the enstatite solid solution. In the pure MgO system (i.e., no CaO, FeO, MnO, etc.), the numerator, the activity of pyrope, is 1, of course, and we may write:

$$\Delta G^o = RT \ln(a_{Mg_2Si_2O_6}\, a_{MgAl_2SiO_6}) = \Delta H^o - T\Delta S^o + (P - P_{ref})\Delta V^o \qquad 4.42$$

(compare equation 4.37). For an ideal case, this may be rewritten as:

$$RT \ln(X_{Mg_2Si_2O_6}\, X_{MgAl_2SiO_6}) = \Delta H^o - T\Delta S^o + (P - P_{ref})\Delta V^o \qquad 4.43$$

Wood and Banno first estimated thermodynamic parameters (ΔH, ΔS, and ΔV for aluminous pyroxene) from experimental data. They dealt with the non-ideality in two ways. First, they assumed ideal solution behavior at 1 bar and assumed all non-ideality associated with substitution of Al in orthopyroxene at higher pressure could be accounted for in the volume term in 4.42, which they rewrote as:

$$\Delta\bar{V}^o = \bar{V}^o_{Mg_3Al_2Si_3O_{12}} - \bar{V}^{o\,opx}_{Mg_2Si_2O_6} - \bar{V}^{o\,opx}_{MgAl_2SiO_6} \qquad 4.44$$

As for non-ideality related to substitution of Ca and Fe in the system, they noted that non-idealities of most silicate systems were of similar size and magnitude and hence the activity coefficients for garnet tend to cancel those for orthopyroxene. Furthermore, the ΔV and ΔH terms are both large and tend to reduce the errors due to non-ideal behavior.

Since equation 4.42 contains temperature as well as pressure terms, it is obvious that the temperature must be known to calculate pressure of equilibration. In the same paper, Wood and Banno (1973) provided the theoretical basis for estimating temperature from the orthopyroxene–clinopyroxene miscibility gap. Thus in a system containing garnet, orthopyroxene and clinopyroxene, both temperature and pressure of equilibration may be estimated from the composition of these phases.

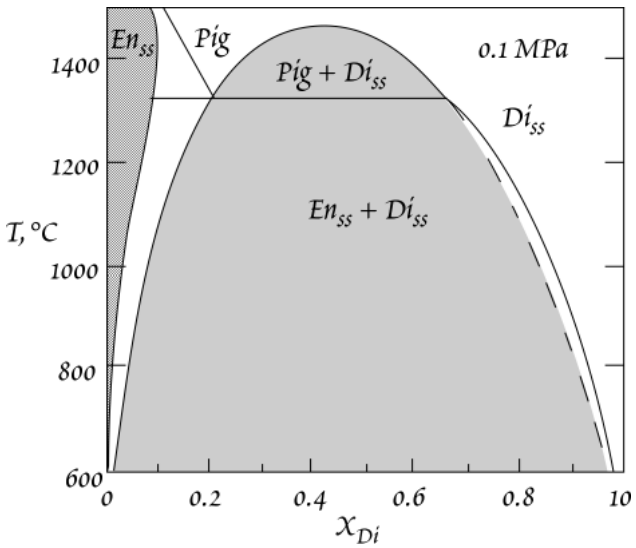

Figure 4.16. Phase relationships in the system $Mg_2Si_2O_6$ (enstatite) — $CaMgSi_2O_6$ (diopside) system (after Lindsley, 1983).

This geobarometer-geothermometer is commonly used to estimate the temperature and pressure (depth) of equilibration of mantle-derived garnet lherzolite xenoliths. One of the first applications was by Boyd (1973), who calculated P and T for a number of xenoliths in South African kimberlites, and hence reconstructed the geotherm in the mantle under South Africa.

4.5.2.2 Solvus Equilibria

Solvus Equilibria provides a second kind of thermobarometer. Generally, these make better geothermometers than geobarometers. A good example is the ortho- and clinopyroxene system, illustrated in Figure 4.16. The two-pyroxene solvus has been the subject of particularly intensive experimental and theoretical work because ortho- and clinopyroxene coexist over a wide range of conditions in Mg, Fe-rich rocks of the crust and upper mantle.

One of the inherent thermodynamic difficulties with this type of geothermometer is that since it involves exsolution, ideal solution models will clearly be very poor approximations. Thus considerable effort has been made to develop solution models for the pyroxenes. Several factors further complicate efforts to use the pyroxene solvus as a thermobarometer. The first is the existence of a third phase, pigeonite (a low-Ca clinopyroxene), at high temperatures and low pressures; the second is that the system is not strictly binary: natural pyroxenes in igneous rocks are solutions of Mg, Ca, and Fe components. The presence of iron is problematic because of the experimental difficulties encountered with Fe-containing systems. These difficulties include the tendency both for iron to dissolve in the walls of commonly used platinum containers and for Fe^{2+} either to oxidize to Fe^{3+} or to reduce to metallic iron, depending on the oxygen fugacity. In addition, other components, particularly Na and Al are often present in the pyroxenes, as we have just seen.

Despite its complexities, the system has been modeled with some success using a symmetric solution model developed by Wood (1987). There are two octahedral sites in both ortho- and clinopyroxenes, generally called M1 and M2. Ca^{2+} occurs only in the M2 site, while Fe and Mg can occupy either site. Ignoring pigeonite and components other than Ca, Mg and Fe, we can treat mixing in the M2 and M1 sites separately. Mixing in the M2 site can be treated as a ternary Mg, Fe, and Ca solution. In a symmetric ternary solution consisting of components A, B, and C, the activities of the components may be calculated from:

$$RT \ln \gamma_A = X_B^2 W_G^{AB} + X_C^2 W_G^{AC} + X_B X_C \left(W_G^{AB} + W_G^{AC} - W_G^{BC} \right) \qquad 4.45$$

where W_G^{AB} is the A-B binary interaction parameter, etc. Mixing of Fe and Mg between the M1 and M2 sites was treated as a simple exchange reaction:

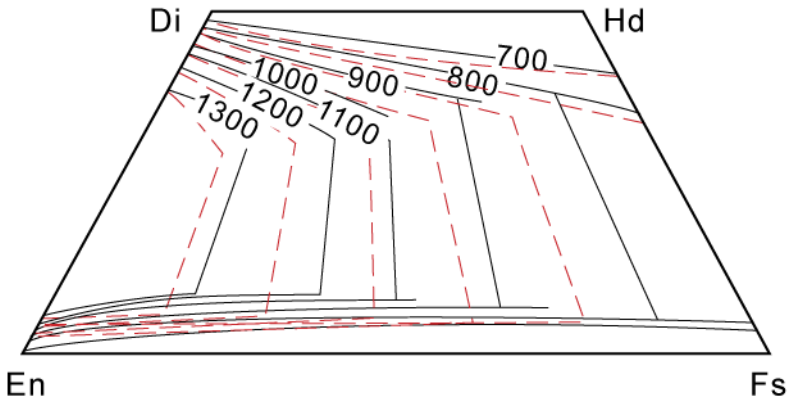

Figure 4.17. Comparison of calculated (solid lines) and experimentally observed (red dashed lines) phase relationships between clino- and orthopyroxene shown in the 'pyroxene quadrilateral', a part of the $CaSiO_3$–$MgSiO_3$–$FeSiO_3$ system. Di: diopside, En: enstatite, Hd: hedenbergite, Fs: ferrosilite. Lines show the limit of solid solution at the corresponding temperatures (° C).

$$Fe_{M2} + Mg_{M1} \rightleftarrows Fe_{M1} + Mg_{M2}$$

with ΔH of 29.27 kJ/mol and ΔS of 12.61 j/mol. Using this approach, Wood calculated the temperature dependence of the solvus in shown in Figure 4.17. The model fits experimental observation reasonably well for the Mg-rich pyroxenes, but significant deviations occur for the Fe-rich pyroxenes.

4.5.2.3 Exchange Reactions

Exchange reaction thermobarometers depend on the exchange of two species between phases. We will consider two examples of these.

The Roeder and Emslie olivine-liquid geothermometer is a rather simple one based on the equilibrium between magma and olivine crystallizing from it. Consider the exchange reaction:

$$MgO_{Ol} + FeO_{liq} \rightleftarrows MgO_{liq} + FeO_{Ol}$$

where *Ol* denotes olivine and *liq* denotes liquid. We can write the equilibrium constant for this reaction as:

$$K_D = \frac{X_{FeO}^{Ol} X_{MgO}^{liq}}{X_{FeO}^{liq} X_{MgO}^{Ol}} \qquad 4.46$$

Recalling our criteria for a good geothermometer, we can guess that this reaction will meet at least several of these criteria. First, olivine exhibits complete solid solution, so we might guess we can treat it as an ideal solution, which turns out to be a reasonably good assumption. We might also guess that the molar volumes of forsterite and fayalite and of their melts will be similar, meaning the ΔV term, and hence pressure dependence, will be small, which is also true. As it turns out, however, the ΔH term, which is related to the difference in heats of fusion of forsterite and fayalite, is also relatively small, so the exchange reaction itself is a poor geothermometer. However, we can consider two separate reactions here:

$$MgO_{liq} \rightarrow MgO_{Ol} \quad \text{and} \quad FeO_{liq} \rightarrow FeO_{Ol}$$

and we can write two expressions for K_D. This was the approach of Roeder and Emslie (1970), who deduced the following relations from empirical (i.e., experimental) results:

$$\log \frac{X_{MgO}^{Ol}}{X_{MgO}^{liq}} = \frac{3740}{T} - 1.87 \qquad 4.47$$

$$\log \frac{X_{FeO}^{Ol}}{X_{FeO}^{liq}} = \frac{3911}{T} - 2.50 \qquad 4.48$$

These K_D's are much more temperature dependent than for the combined exchange reaction. Subtracting equation 4.47 from 4.48 yields:

$$\log K_D = \frac{171}{T} - 0.63$$

where K_D is defined as in equation 4.46. Note that these equations have the form of equation 3.95. Roeder and Emslie

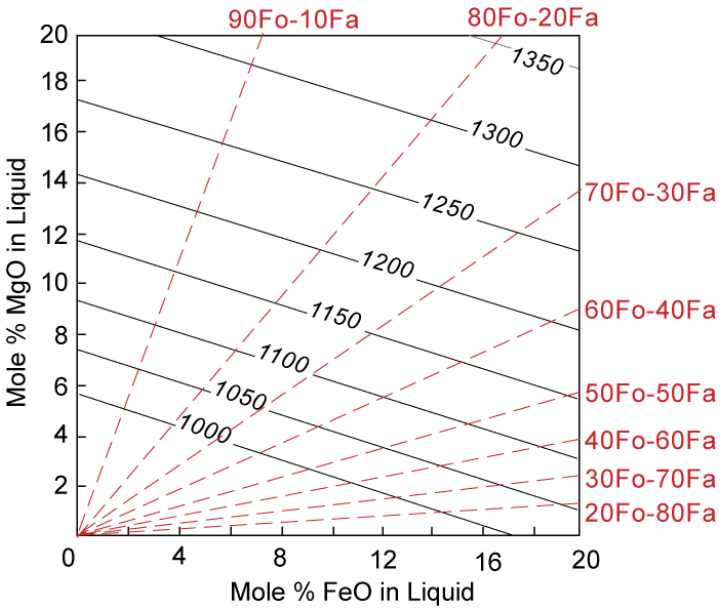

Fig. 4.18. Olivine saturation surface constructed by Roeder and Emslie (1970).

(1970) used these equations to construct the diagram in Figure 4.18.

The iron-titanium oxide system evaluated by Buddington and Lindsley (1964) was one of the first means of obtaining quantitative estimates of crystallization temperatures of igneous rocks. It is important not only because it is useful over a wide range of temperatures and rock types, but also because it yields oxygen fugacity as well. Figure 4.19 shows the TiO_2–FeO–Fe_2O_3 (rutile–wüstite–hematite) ternary system. The geothermometer is based on the reaction:

Example 4.3. Calculating Magma Temperatures Using the Olivine Geothermometer

From the electron microprobe analysis of glass of a mid-ocean ridge basalt and its coexisting olivine microphenocryst, calculate the temperature at which the olivine and liquid equilibrated:

SiO_2	50.3
Al_2O_3	14.3
ΣFeO	11.1
MgO	7.2
CaO	11.5
Na_2O	2.6
K_2O	0.23
MnO	0.20
TiO_2	1.71
Total	99.02
Mol % Fo in Ol	82

Answer: We will answer this assuming the glass composition represents that of the liquid and using equations 4.47 and 4.48. To use the equations, we will have to convert the analysis of the glass from weight percent to mole fraction.

Let's setup a spreadsheet to do these calculations. First we must deal with the Fe analysis. The analysis reports only iron as FeO. Generally, about 10% of the iron in a basaltic magma will be present as ferric iron (Fe_2O_3), so we will have to assign 10% of the total iron to Fe_2O_3. To do this, we get the weight percent FeO simply by multiplying the total FeO by 0.9. To get weight percent Fe_2O_3, we multiply total FeO (11.1%) by 0.1, then multiply by the ratio of the molecular weight of Fe_2O_3 to FeO and divide by 2 (since there are 2 Fe atoms per 'molecule').

	wt%	w/10% ferric	Mol. wt	moles	mol frac.
SiO2	50.3	50.3	60.09	0.8371	0.5265
Al2O3	14.3	14.3	102	0.1402	0.0882
total FeO	11.1	11.1			
FeO		9.99	71.85	0.1390	**0.0875**
Fe2O3		1.22	157.7	0.0077	0.0049
MgO	7.8	7.8	40.6	0.1921	**0.1208**
CaO	11.5	11.5	56.08	0.2051	0.1290
Na2O	2.6	2.6	61.98	0.0419	0.0264
K2O	0.23	0.23	94.2	0.0024	0.0015
MnO	0.2	0.2	70.94	0.0028	0.0018
TiO2	1.71	1.71	79.9	0.0214	0.0135
Total	99.74	99.85		1.590	1.000
XMgO-Ol					**0.82**
XFeO-Ol					**0.18**
	TMgO	**1384**	**kelvin**	**1111**	**°C**
	TFeO	**1390**	**kelvin**	**1117**	**°C**

Now we are ready to calculate the mole fractions. We'll set up a column with molecular weights and divide each weight percent by the molecular weight to get the number of moles per 100 grams. To convert to mole fraction, we divide the number of moles by the sum of the number of moles.

Since the mole fraction of Mg in olivine is equal to the mole fraction of forsterite, we need only convert percent to fraction (i.e., divide by 100). The mole fraction of FeO in olivine is simply $1 - X_{MgO}$. Thus $X_{MgO\ (ol)} = 0.82$ and $X_{FeO\ (ol)} = 0.18$. Now we are ready to calculate temperatures. We can calculate 2 temperatues: one from MgO, and the other from FeO. The temperature based on the FeO exchange is:

$$y\mathrm{Fe_2TiO_4} + (1\text{-}y)\mathrm{Fe_3O_4} + \frac{1}{4}\mathrm{O_2} \rightleftarrows y\mathrm{FeTiO_3} + \left(\frac{3}{2}\text{-}y\right)\mathrm{Fe_2O_3} \qquad 4.50$$

which describes equilibrium between the ulvospinel–magnetite (titanomagnetite) and ilmenite–hematite solid solution series. The equilibrium constant expression may be written as:

$$\mathrm{K} = \frac{a_{FeTiO_3}^{y} a_{Fe_2O_3}^{3/2-y}}{a_{Fe_2TiO_4}^{y} a_{Fe_3O_4}^{1-y} f_{O_2}^{1/4}} \qquad 4.51$$

The original Buddington and Lindsley geothermometer was based on empirica observations of compositional dependence on oxygen fugacity and temperature, as shown in Figure 4.20. Having values for the compositions of the titanomagnetite and ilmenite phases, one simply read T and f_{O_2} from the graph. To understand the system from a thermodynamic perspective, it is better to consider the two fundamental reactions occurring separately in this system:

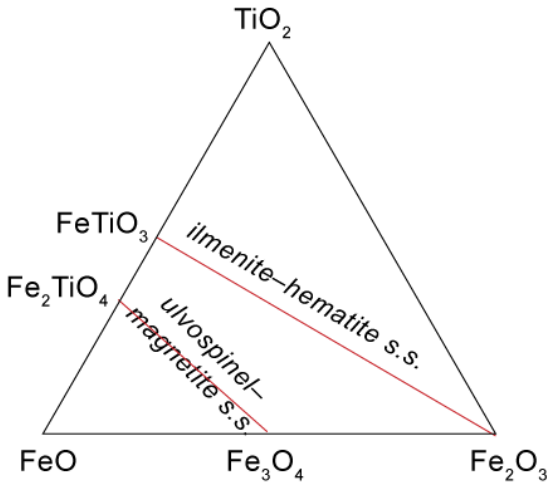

Figure 4.19. The TiO_2–FeO–Fe_2O_3 ternary system. Phases are: FeO: wüstite; Fe_2O_3: hematite; TiO_2: rutile; Fe_2TiO_4: ulvospinel; Fe_2O_4: magnetite; $FeTiO_3$: ilmenite. The system also includes the $FeTi_2O_5$—Fe_2TiO_5 solution, which is not shown.

$$\mathrm{Fe_3O_4} + \mathrm{FeTiO_3} \rightleftarrows \mathrm{Fe_2TiO_4} + \mathrm{Fe_2O_3} \qquad 4.52$$

$$\text{Magnetite} + \text{Ilmenite} \rightleftarrows \text{Ulvospinel} + \text{Hematite}$$

and:

$$4\mathrm{Fe_3O_4} + \mathrm{O_2} \rightleftarrows 6\mathrm{Fe_2O_3} \qquad 4.53$$

The first reaction represents a temperature dependent exchange between the titanomagnetite and ulvospinel solutions; the second reaction is the oxidation of magnetite to hematite.

Several investigators have studied the iron-titanium oxides attempting to improve upon the work of Buddington and Lindsley (1964). The approach of Spencer and Lindsley (1981) was to consider two reactions 4.52 and 4.53. They modeled the ilmenite as a binary asymmetric Margules solution and titanomagnetite as a binary asymmetric Margules solution below 800° C and as an ideal binary solution above 800° C. They modeled configurational entropy based ordering of Fe^{2+}, Fe^{3+}, and Ti^{4+} in the ilmenite lattice structure (they assumed Fe^{3+} mixed randomly with Ti^{4+} in 'A' sites and Fe^{3+} and Fe^{2+} randomly in 'B' sites). The ΔG of reactions above were written as:

$$-\frac{\Delta G^\circ}{RT} = \ln\left[\frac{X_{Usp}^{\alpha}(1-X_{Ilm})^{\alpha}}{(1-X_{Usp})^{\alpha} X_{Ilm}^{\alpha}}\right] + \ln\left[\frac{\lambda_{Usp}^{\alpha}\lambda_{Hem}^{\alpha}}{\lambda_{Mt}^{\alpha}\lambda_{Ilm}^{\alpha}}\right] \qquad 4.54$$

and:

$$-\frac{\Delta G}{RT} = \ln\left[\frac{X_{Hem}^{6\alpha}}{X_{Mt}^{4\alpha}}\right] + \ln\left[\frac{\lambda_{Hem}^{6\alpha}}{\lambda_{Mt}^{6\alpha}}\right] - \ln f_{O_2} \qquad 4.55$$

The α parameter is related to the number of sites involved in the exchange; Spencer and Lindsley assumed α was 2 for ilmenite and 1 for titanomagnetite. The excess free energy was expressed in the usual way for an asymmetric solution (equation 4.16):

$$\bar{G}_{ex} = \left(W_{G_1} X_2 + W_{G_2} X_1\right) X_1 X_2$$

for each solution series. When the effect of pressure is neglected, the free energy interaction parameter expression (equation 4.08) simplifies to:

$$W_G = W_H - TW_S \qquad 4.56$$

Values for W_H and W_S were obtained from least-squares fits to experimental data. The parameters obtained are listed in Table 4.1.

Substituting equations 4.56 and 4.16 into the free energy of solution expression ($\Delta G_{excess} = \Delta G_{ideal} - \Delta G_{real}$), the following equation can be obtained:

$$T(K) = \frac{AW_H^{Usp} - BW_H^{Mt} - CW_H^{Il} + DW_H^{Hem} + \Delta H^o}{AW_S^{Usp} - BW_S^{Mt} - CW_S^{Il} + DW_S^{Hem} + \Delta S^o - R\ln K^{exch}} \qquad 4.57$$

Oxygen fugacity is determined as:

$$\log f_{O_2} = \log MH + \left(\begin{array}{l} 12\ln(1-X_{ilm}) - 4\ln(1-X_{Usp}) + \\ \frac{1}{RT}\left[\begin{array}{l} 8X_{Usp}^2(X_{Usp}-1)W_G^{Usp} + 4X_{Usp}^2(1-2X_{Usp})W_G^{Mt} + \\ 12X_{Ilm}^2(1-X_{Ilm})W_G^{Ilm} - 6X_{Ilm}^2(1-2X_{Ilm})W_G^{Hem} \end{array} \right] \end{array} \right) \Big/ 2.303 \qquad 4.58$$

where:

$A = 3X_{Usp}^2 - 4X_{Usp} + 1$, $B = 3X_{Usp}^2 - 2X_{Usp}$, $C = 3X_{Ilm}^2 - 4X_{Ilm} + 1$, $D = 3X_{Ilm}^2 - 2X_{Ilm}$

$K^{exch} = (X_{Usp}X_{Hem}^2) \Big/ (X_{Mt}X_{Ilm}^2)$, $\Delta H^o = 27.799$ kJ/mol, $\Delta S^o = 4.1920$ J/K-mol

and MH is the magnetite-hematite buffer: $\log MH = 13.966 - 24634/T$.

We have reviewed just a few of the available thermobarometers in use. These were selected to illustrate the underlying principles. There are, however, many thermobarometers in use by geochemists and petrologists. Some of these are listed in Table 4.2.

Table 4.01. Margules Parameters for Ilmenite and Titanomagnetite Solid Solutions

	Usp (<800 ° C)	Mag (<800° C)	Ilm	Hem
W_H (joules)	64835	20798	102374	36818
W_S (joules)	60.296	19.652	71.095	7.7714
W_G (>800° C) (joules)	0	0		
ΔS^o_{Usp} (joules)	4.192			
ΔH^o_{Usp} (joules)	27799			

EXAMPLE 4.4: USING THE IRON-TITANIUM OXIDE GEOTHERMOMETER

An electron microprobe analysis of oxide phases in an andesite reveals that there is 68 mole percent of ulvospinel in an ulvospinel–magnetite phase and 93.3% of ilmenite in an illmenite-hematite phase. Calculate the temperature and fO_2 at which these phases equilibrated.

Answer: We can use equations 4.57 and 4.58 to answer this question. The data in Table 4.2 are relevant to the binary asymmetric solution model for the system below 800° C. Above 800° C, an ideal solution is assumed for the ulvospinel-magnetite phase, so the interaction parameters for this phase go to 0. But if we don't know the temperature, how do we know which equation to use? We begin by computing temperature using the parameters for less than 800° C. If the temperature computed in this way is greater than 800° C (1073 K), we set the W_H and W_S for ulvospinel and magnetite to 0 and recompute.

Once we have temperature, we can compute the W_G terms using the relationship $W_G = W_H - TW_S$, bearing in mind that $W_{G_{usp}} = W_{G_{Mt}} = 0$ if the temperature is greater than 800° C. With these values in hand, we can use equation 4.58 to calculate the fO_2. Our spreadsheet is shown on the right. These data we taken from one of Spencer and Lindsley's (1981) experiments, performed at 938° C and log fO_2 = -12.76. Our calculations are in good agreement with the experimental observation.

	XUsp	XIlm			
	0.68	0.933			
	ΔH	27799			
	ΔS	4.192			
	R	8.314			
	Interaction Parameters				
	WHU	64835	WSU	60.296	
	WHM	20798	WSM	19.652	
	WHI	102374	WSI	71.095	
	WHH	36818	WSH	7.7714	
	A	-0.3328			
	B	0.0272			
	C	-0.12053			
	D	0.745467			
	K	0.010958			
T=	(A*WHU-B*WHM-C*WHI+D*WHH+ΔH)				
	(A*WSU-B*WSM-C*WSI+D*WSH+ΔS-R*ln(K)				
T (<800)		1281	K	1008	°C
T (>800)		1205	K	932	°C
	WG=WH-T*WS				
	WGU	-7829.52	WGI	16695.29	
	WGM	-2885.21	WGH	27452.45	
			MH	-6.47	
		Log$fO2$ (<800)		-12.58	
		Log$fO2$ (>800)		-12.69	

4.6 THERMODYNAMIC MODELS OF MAGMAS

Silicate liquids have played an extremely important role in the development of the Earth, as well as other bodies in the solar system. As we shall see, the Earth's crust formed as melts from the mantle rose to the surface and cooled. Thus an understanding of igneous processes is an essential part of earth science. Until the a few decades ago, the primary approaches to igneous petrology were observational and experimental. Results of melting experiments in the laboratory were used to interpret observations on igneous rocks. This approach proved highly successful and is responsible for most of our understanding igneous processes. However, such an approach has inherent limitations: virtually every magma is unique in its composition and crystallization history. Yet the experimental database is limited: it is not practical to subject each igneous rock to melting experiments in the laboratory. Realizing this, igneous petrologists and geochemists turned to thermodynamic models of silicate melts as a tool to interpret their evolution. With a proper 'model' of the interaction of various components in silicate melts and adequate thermodynamic data, it should be possible to predict the equilibrium state of any magma under any given set of conditions. The obstacles in developing proper thermodynamic models of silicate liquids, however, have been formidable. Because they are stable only at high temperatures,

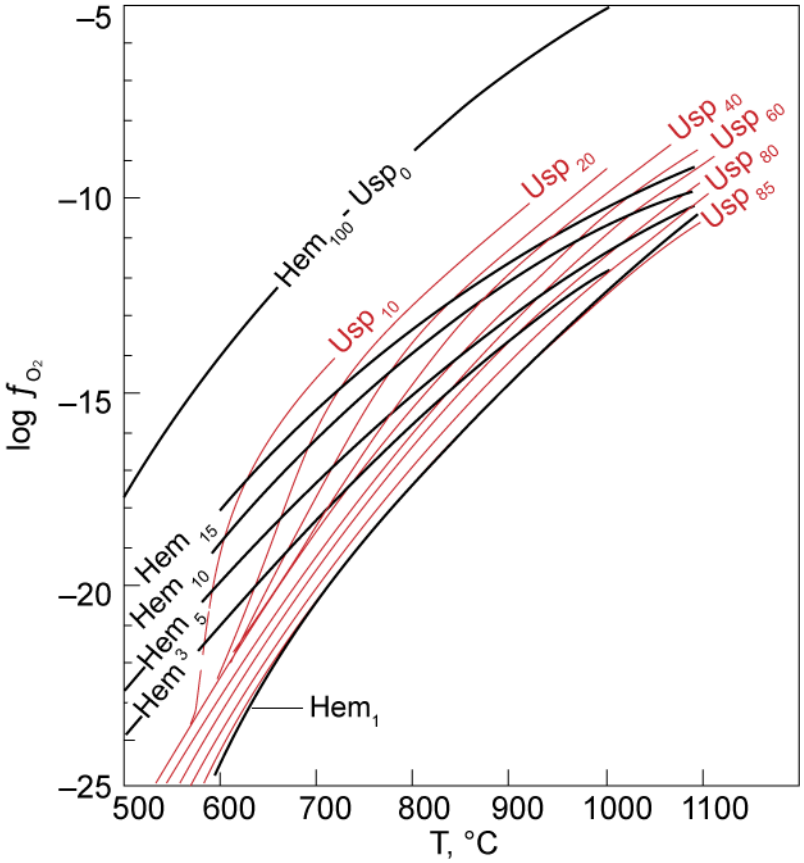

Figure 4.20. Relationship of composition of coexisting titanomagnetite and ilmenite to temperature and oxygen fugacity.

consider the nature of silicate melts on the atomic level.

obtaining basic thermodynamic data on silicate liquids is difficult. Furthermore, silicate liquids are very complex solutions, with 8 or more elements present in high enough concentrations to affect the properties of the solution. Nevertheless, sufficient progress has been made on these problems that thermodynamics is now an important tool of igneous petrology.

4.6.1 Structure of Silicate Melts

As was the case for silicate solids and electrolyte solutions, application of thermodynamics to silicate liquids requires some understanding of the interactions that occur on the atomic level. Thus we will once again have to consider the microscopic viewpoint before developing a useful thermodynamic approach. In this section, we briefly

Table 4.02. Commonly Used Thermobarometers

Reaction	Type	Reference
Garnet=Biotite Fe-Mg $(Fe,Mg)_3Al_2Si_3O_{12} \rightleftarrows K(Mg,Fe)AlSi_3O_{10}(OH)_2$	exchange	(Ferry and Spear, 1978)
Plagioclase = Garnet + Kyanite + Quartz $3(Ca,Na)Al_2Si_2O_8 \rightleftarrows (Fe,Ca)_3Al_2Si_3O_{12} + 2Al_2SiO_5 + SiO_2$	displaced equilibria	(Ghent, 1976; Koziol and Newton, 1988)
Garnet + Quartz = Plagioclase + Wollastonite $(Fe,Ca)_3Al_2Si_3O_{12} + SiO_2 \rightleftarrows (Ca,Na)Al_2Si_2O_8 + 2CaSiO_3$	displaced equilibria	(Gasparik, 1984b)
Calcite = Dolomite $CaCO_3 \rightleftarrows (Ca,Mg)CO_3$	solvus equilibria	Goldsmith and Newton (1978)
Calcite = Aragonite $CaCO_3 \rightleftarrows CaCO_3$	univariant	(Johannes and Puhan, 1971)
Ilmenite + Al_2SiO_5 = Garnet + Rutile + Quartz $3FeTiO_3 + Al_2SiO_5 \rightleftarrows 3TiO_2 + (Fe,Ca)_3Al_2Si_3O_{12} + SiO_2$	displaced equilibria	(Bohlen et al., 1983)
Hercynite + Quartz = Garnet + Sillimanite $FeAl_2O_4 + 5SiO_2 \rightleftarrows Fe_3Al_2Si_3O_{12} + Al_2SiO_5$	displaced equilibria	(Bohlen et al., 1986)

Chapter 4: Applications of Thermodynamics

Most, though not all, of our knowledge of the structure has come from studies of glasses rather than melts. While the thermodynamic properties of silicate liquids and their respective glasses differ, other studies have confirmed the general structural similarities of glasses and liquids. Spectral studies of glasses, which in some respects can be viewed as supercooled liquids, have revealed that silicate liquids have structures rather similar to those of silicate solids. In fact, the principal difference between silicate liquids and solids is the absence of long-range ordering in the former; short range ordering is similar. As in silicate minerals, the primary structural element of silicate liquids is the silicon tetrahedron (see Fig. 1.11), consisting of a silicon atom surrounded by four oxygens. As in silicate minerals, tetrahedra may be linked by a shared oxygen, called a *bridging* oxygen; not surprisingly, unshared oxygens are termed *non-bridging* (Figure 4.21a). Unlinked silica tetrahedra, that is, those with no bridging oxygens, are termed monomers, SiO_4^{4-} (Figure 4.21b). Two tetrahedra linked by a single oxygen are termed *dimers* and have the formula $Si_2O_7^{6-}$. Tetrahedra may also be linked by two oxygens to form infinite chains; these have a chemical formula of SiO_3^{2-}.In silicates such as quartz and feldspar, the tetrahedra are all linked into a framework, and all oxygens are shared. All these structural elements can be present in silicate glasses.

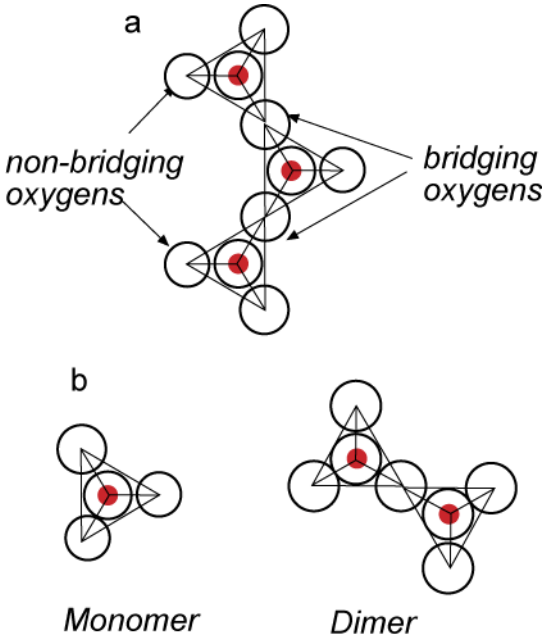

Figure 4.21. Silicate structures. a: Short range silicate structures in melts resemble those in solids. Individual tetrahedra may be linked by bridging oxygens and linked to 2 silicon atoms. b. Unit in silicate melts may include monomers, with no bridging oxygens, and dimers, where only 1 of 4 oxygens in each tetrahedra are 'bridging'.

The degree to which the silica tetrahedra are linked, or *polymerized*, in silicate liquids affects chemical and physical properties. The degree of polymerization in turn depends on other cations present. These may be divided into two groups, *network formers* and *network modifiers*. Relatively small, highly charged cations such Al^{3+} and Fe^{3+} (more rarely, Ti^{4+}, P^{3+}, B^{3+} as well) often substitute for silicon in tetrahedral sites and, along with Si, are termed *network formers*. The other common cations of natural silicate liquids, Ca^{2+}, Mg^{2+}, K^+, Na^+, and H^+, are network modifiers. These ions cannot substitute for silicon in tetrahedra and their positive charges can only be balanced by non-bridging oxygens. Addition of these ions disrupts the linkages between silica tetrahedra. Thus as silicate melts become richer in these network modifiers they become progressively depolymerized. This is illustrated in Figure 4.22, which compares the structure of pure silica glass (liquid) and a silica-rich glass (liquid). Melt structure in turn affects the physiochemical properties of the melt. For example, SiO_2–rich melts tend to have low densities and high viscosities. As ions such as MgO or CaO are added to the melt, viscosity decreases and density increases as the polymer structure is disrupted.

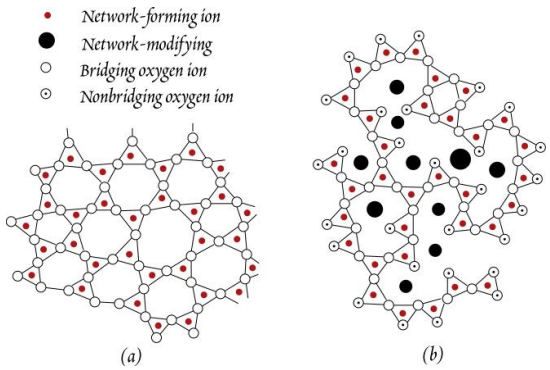

Figure 4.22. (a) structure of pure silica glass and (b) a silica-rich glass with additional component ions.

4.6.2 Magma Solution Models

Advances on several fronts have moved thermodynamic modeling of magmas from an academic curiosity to a useful petrological tool. First, spectroscopic (mainly Raman and infrared spectroscopy, both of which are sensitive to atomic and molecular vibrations) studies are revealing the structure of silicate melts, which provides the theoretical basis for thermodynamic models. Second, more sophisticated thermodynamic models more accurately reflect interactions in silicate melts. Third, the thermodynamic database has become more complete and more accurate. Finally, the wide accessibility and power of computers and appropriate programs have made the extensive matrix calculations involved in these models possible.Several factors complicate the task of thermodynamic modeling of magmas. First, magmas are solutions of many components (typically 8 or more). Second, the solids crystallizing from magmas are themselves solutions. Third, magmas crystallize over a substantial temperature range (as much as 400-500° C, more in exceptional cases). Furthermore, crystallization may occur over a range of pressures as a magma ascends through the Earth, and crystallization may be accompanied by melting and assimilation of the surrounding 'country' rock. Despite these complications several models that are sufficiently accurate to be useful to petrologists have been published, most notably those of Ghiorso (Ghiorso et al., 1983; Ghiorso and Sack, 1995) and Nielsen and Dungan (1983). The goal of these models is to describe the phases and their proportions in equilibrium with a magma, and the resulting evolution of liquid composition. In particular the models of Ghiorso and colleagues are applicable to both melting and crystallization. In the section below, we briefly consider the model of Ghiorso.

4.6.2.1 The Regular Solution Model of Ghiorso and Others: "MELTS"

Ghiorso (Ghiorso et al., 1983; Ghiorso, 1987; Ghiorso and Sack, 1995; Ghiroso et al. (2002) noted that silicate liquids have substantial compositional regions in which immiscibility occurs and therefore argued that the simplest model that might be able to describe them is the regular solution model. As we saw earlier in the chapter, regular solution models attempt to describe excess functions with interaction, or Margules, parameters. The Margules equation for excess Gibbs Free Energy for many components is:

$$\overline{G}_{ex} = \frac{1}{2}\sum_i \sum_{j,j\neq i} X_i X_j W_G^{i,j} \qquad 4.59^*$$

and the Gibbs Free Energy is:

$$\overline{G} = \sum X_i \mu_i^o + RT\sum_i X_i \ln X_i + \frac{1}{2}\sum_i \sum_j X_i X_j W_G^{i,j} \qquad 4.60^\dagger$$

The chemical potentials of individual components are:

$$\mu_i = \mu_i^o = +RT \ln X_i + \sum_{j,j\neq i} X_j W_G^{i,j} - \frac{1}{2}\sum_{j,j\neq k}\sum_{k,k\neq j} X_j X_k W_G^{j,k} \qquad 4.61$$

and the activity coefficients are:

$$RT \ln \lambda_i = \sum_j X_j W_G^{i,j} - \frac{1}{2}\sum_j \sum_k X_j X_k W_G^{j,k} \qquad 4.62$$

Having chosen a general form for the solution model, the next step is to select the components. For practical reasons, Ghiorso et al. (1983) placed all components on an 8-oxygen basis. Ghiorso and Sack (1995) chose liquid components that were "mineral-like": SiO_2, TiO_2, Al_2O_3, Fe_2O_3, $MgCr_2O_4$, Fe_2SiO_4, Mg_2SiO_4, $CaSiO_3$, $KAlSiO_4$, etc. and H_2O. For components of solid phases, they chose pure end-member

---

* The $\frac{1}{2}$ term arises because the sum contains both $X_i X_j W_G^{ij}$ and $X_j X_i W_G^{ij}$ terms and $W_G^{ij} = W_G^{ji}$.

† For clarity, we have simplified Ghiorso's equation by neglecting H_2O, which they treated separately.

phase components (e.g., $MgSiO_3$ in orthopyroxene). The problem with this approach is that the concentrations of these components varied greatly; for example, the mole fraction of SiO_2 is typically 0.4 in basaltic magmas where as that of Mg_2SiO_4 is typically less than 0.1 and that of $KAlSiO_4$ is typically less than 0.05. We can see from equation 4.60 that when X_i is small, the contribution of the interaction parameters for this component, $W_G^{i,j}$ to the free energy will also be small. Consequently, in the most recent version of this model, called *pMELTS*, Ghiroso et al. (2002) redefined the liquid components so that their mole fractions were more similar, e.g., $SiO_2 \rightarrow Si_4O_8$, $Na_2SiO_3 \rightarrow NaSi_{0.5}O_{1.5}$, etc.

The next task is to find values for the interaction parameters. These can be calculated from solid-liquid equilibria experiments. The principle involved is an extension of that which we used in constructing phase diagrams: when a solid and liquid are in equilibrium, the chemical potential of each component in each phase must be equal. Since thermodynamic properties of the solids involved are available (determined using standard thermodynamics techniques), the thermodynamic properties of the coexisting liquid may be calculated.

The reaction of a solid phase, φ, with the melt can be described with a set of p reactions of the form:

$$\varphi_p \rightleftarrows \sum_i \nu_{p,i} c_i \qquad 4.63$$

where φ_p is the p^{th} end member component of phase φ, c_i refers to the formula for the i^{th} component in the liquid and $\nu_{p,i}$ refers to the stoichiometric coefficient of this component. Thus for reaction of olivine with the liquid, we have two versions of 4.63:

$$(Mg_2SiO_4)_{Ol} \rightleftarrows 2MgO_\ell + SiO_{2\text{-}\ell} \qquad 4.63a$$

and

$$(Fe_2SiO_4)_{Ol} \rightleftarrows 2FeO_\ell + SiO_{2\text{-}\ell} \qquad 4.63b$$

We can express the Gibbs Free Energy change for each of these reaction as:

$$\Delta\bar{G}_r = \Delta\bar{G}^o_{\varphi_p} + RT\sum_i \nu_{p,i} \ln a_i^\ell - RT \ln a_{\varphi_p} \qquad 4.64$$

where a_i^ℓ is the activity of the oxide component in the liquid and φ_p refers to phase component p in phase φ. $\Delta\bar{G}_r$ is, of course, 0 at equilibrium. For example, for reaction 4.63a above, we have:

$$\Delta\bar{G}_r = 0 = \Delta\bar{G}^o_{Fo} + RT\left[2\ln a^\ell_{MgO} + \ln a^\ell_{SiO_2}\right] + RT\ln a_{Fo}$$

where the subscript *Fo* refers to the forsterite (Mg_2SiO_4) component in olivine and the superscript ℓ refers to the liquid phase. Expanding the liquid activity term, we have:

$$0 = \Delta\bar{G}^o_{\varphi_p} + RT\sum_i \nu_{p,i} \ln X_i^\ell + RT\sum_i \nu_{p,i} \ln \lambda_i^\ell - RT \ln a_{\varphi_p} \qquad 4.65$$

Substituting 4.62 for the activity coefficient term in 4.65 and rearranging to place the "knowns" on the left-hand side, we have:

$$-\Delta\bar{G}^o_{\varphi_p} + RT\ln a_{\varphi_p} - RT\sum_i \nu_{p,i} \ln X_i^\ell = \sum_i \nu_{p,i} \sum_j X_j W_G^{i,j} - \frac{1}{2}\sum_j \sum_{k,k\neq j} X_k X_j W_G^{k,j} \qquad 4.66$$

The quantities on the left-hand side of the equation are terms that can be calculated from the compositions of coexisting solids and liquids and solution models of the solids. The right hand side contains the unknowns. One statement of equation 4.66 can be written for each component in each solid phase at a given temperature and pressure. With enough experiments, values for the interaction parameters can be extracted from the phase relations. Ghiorso et al. (1983) and Ghiorso and Sack (1995) used a statistical technique called least squares† to determine the interaction parameters from a large number of

† 'Least squares' is a numerical technique that attempts to minimize the square of the difference between calculated and observed value of some parameter. The square is taken to give greater weight to large deviations. Thus least squares techniques yield results where there are relatively few large deviations between the calculated and observed value of the parameter of interest. We discuss this technique further in Chapter 8.

Table 4.03. Interaction Parameters for the Ghiorso Regular Solution Model

	SiO_2	TiO_2	Al_2O_3	Fe_2O_3	$MgCr_2O_4$	Fe_2SiO_4	Mg_2SiO_4	$CaSiO_3$	Na_2SiO_3	$KAlSiO_4$	$Ca_3(PO_4)$
TiO_2	26267										
Al_2O_3	--39120	-29450									
Fe_2O_3	8110	-84757	-17089								
$MgCr_2O_4$	27886	-72303	-31770	21606							
Fe_2SiO_4	23661	5209	-30509	-179065	-82972						
Mg_2SiO_4	3421	-4178	-32880	-71519	46049	-37257					
$CaSiO_3$	-864	-35373	-57918	12077	30705	-12971	-31732				
Na_2SiO_3	-99039	-15416	-130785	-149662	113646	-90534	-41877	-13247			
$KAlSiO_4$	-33922	-48095	-25859	57556	75709	23649	22323	-17111	6523		
$Ca_3(PO_4)_2$	613892	25939	52221	-4214	5342	87410	-23209	37070	15572		
H_2O	30967	81879	-16098	31406		28874	35634	20375	--96938	10374	43451

Values are in kJ/mol. From Ghiorso and Sack (1995).

published experimental data. Ghiorso and Sack (1995) also noted that the absence of a phase in an experiment provides thermodynamic information about that phase, i.e., that its free energy must be higher than that of the phases that are present. Their approach made use of this information as well, though discussion of that aspect of their method would take us too far afield. In all, Ghiroso and Sack (1995) used data from 1593 published laboratory experiments. The interaction parameters they determined are listed in Table 4.3. In constructing the *pMELTS* model, Ghiroso et al. (2002) used mineral-liquid equilibrium constraints derived from published results of 2439 different laboratory experiments.

One of the goals of the *pMELTs* was to improve the thermodynamic predictions at higher pressures. Since many melting reactions involve significant volume changes, this required an improved equation of state for the liquid, i.e., an improved description of the relationship between volume and pressure. Ghiroso et al. (2002) chose a third order Birch-Murnaghan equation:

$$P = \frac{3}{2}K\left[\left(\frac{V^\circ}{V}\right)^{\frac{1}{3}} - \left(\frac{V^\circ}{V}\right)^{\frac{5}{3}}\right]\left\{1 - \frac{3}{4}(4 - K')\left[\left(\frac{V^\circ}{V}\right)^{\frac{3}{2}} - 1\right]\right\} \qquad 4.67$$

where K is the bulk modulus. New experimental data on density derived from new shock wave experiments and new experimental determinations of silicate liquid density (by suspending olivine crystals in the liquid and observing if they sink or float) were used to constraint the K' parameter. A new equation of state for water was also incorporated into *pMELTS*.

With values for the interaction parameters, the model can then be used to predict the assemblage of solids, their compositions, and the liquid composition that will be present in the system as a function of temperature and pressure. The equilibrium condition for a magma, as for any other system, is the condition where Gibbs Free Energy is at a minimum. Thus the problem becomes finding compositions for the liquid and coexisting solids that minimizes G at a particular temperature and pressure. In other words, we want to find values of G_ℓ and $G_{\phi 1}$, $G_{\phi 2}$, ... $G_{\phi n}$ such that G_{sys} is minimal where:

$$G_{sys} = G_\ell + \sum_\varphi G_\varphi \qquad 4.68$$

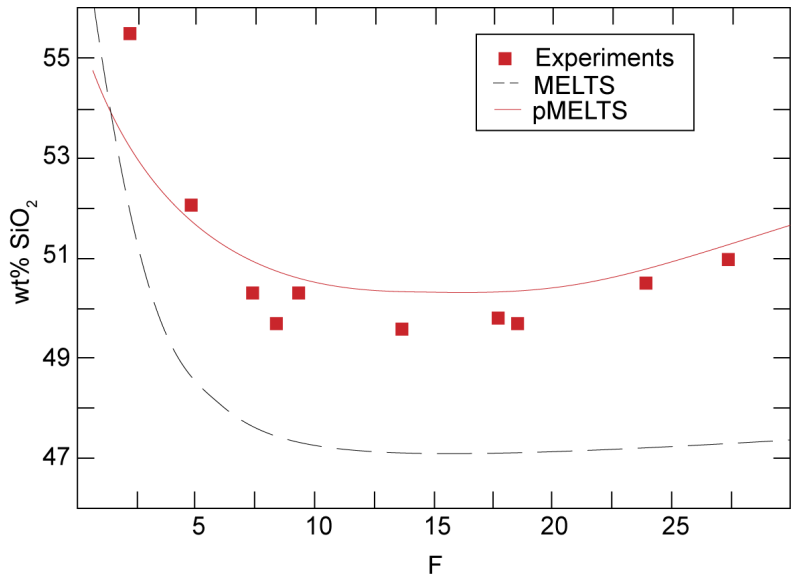

Figure 4.23. SiO_2 concentrations in a melt produced by melting of peridotite at 1 GPa as a function of *F*, the percent fraction of melt in the system. Figure compares the predictions of the earlier version of the MELTS model, the newer version, pMELTS, and experimentally determined composition. After Ghiroso et al. (2002).

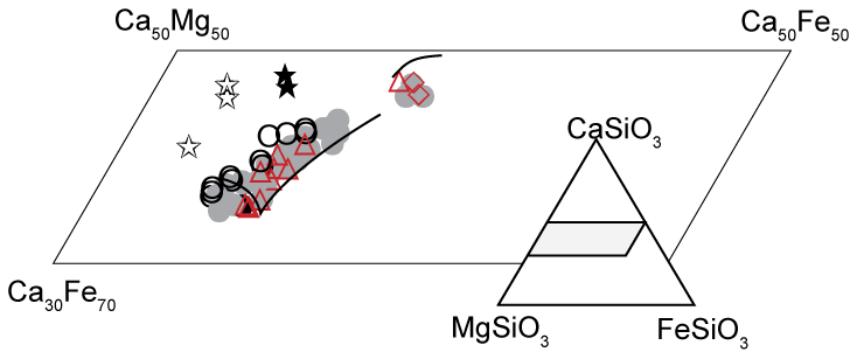

Figure 4.24. Compositions of pyroxenes found in lavas from two the Cameroon Line. Diamonds, circles, and triangles are *megacrysts* and likely to have crystallized from these lavas. Stars are pyroxenes in *xenoliths* accidentally incorporated in the lavas. Lines show the compositions of the pyroxenes predicted by *pMELTS* to crystallize from these magmas as they cool and evolve. After Rankenburg et al. (2004).

Inherent in the problem is finding which solids will be in equilibrium with the liquid for a given bulk system composition at specified temperature and pressure. In Ghiorso's approach, an initial guess is made of the state of the system. This is done by taking the liquid composition as equal to the system composition and estimating what phases are likely to be in equilibrium with this liquid. Then G is expanded as a 3-term Taylor Series[‡] about that initial point, N', where N' is the composite vector containing the mole fractions describing the compositions of all phases in the system. The second term in the expansion is the matrix of first derivatives of G with respect to n_i, the moles of component *i*, which is simply the matrix of the chemical potentials. A minimum of G occurs where the first derivative is 0. Thus the second term is set to 0 and solution sought by successive iterations. After each iteration N' is reset to the composition found in the most recent iteration. This approach clearly involves repetitive matrix calculations and would not be practical without a computer, but they can easily be performed on the current generation of computers.

The goal of a thermodynamic model such as MELTS is to predict the both the composition of the melt and composition of coexisting solid phases if temperature, pressure and the composition of the system can be specified. Thus such a program should be able to

[‡] A Taylor series expansion of a function $f(z)$ in the vicinity of some point z = a has the form:

$$f(z) = f(a) + \frac{(z-a)}{1!} f'(a) + \frac{(z-a)^2}{2!} f''(a) + \ldots$$

where f' and f'' are the first and second derivatives of f with respect to z.

predict the composition of the melt generated in a region undergoing melting and how the composition of that melt evolves as it rises and cools nearer the surface. Figure 4.23 compares the predictions of the 1995 and 2002 versions of the model with experimentally determined compositions of the liquid produced by melting peridotite at 1 GPa. The agreement between the model and experimental observation is clearly improved in *pMELTS*, but it is also clear the predictions still do not agree perfectly with observations.

Figure 4.24 compares the compositions of clinopyroxene crystals found in basaltic lavas of Cameroon Line volcanoes with the compositions predicted by *pMELTS* to crystallize from these magmas. Diamonds and circles are *megacrysts*, and are likely to have crystallized from the magmas. Stars are pyroxenes in ultamafic xenoliths, which are more likely pieces of mantle accidentally incorporated in the magma. The kink in the lower link reflects the onset of garnet crystallization. The agreement is not perfect but this diagram nevertheless shows the enormous value of the this thermodynamic approach in igneous petrology. In this example, Rankenburg et al. (2004) were able to estimate the pressue and temperature of crystallization as 1400˚C and 1.7-2.3 GPa. These pressures correspond to depths greater than the thickness of the crust in this area, hence the authors concluded the pyroxene megacrysts must have crystallized in the mantle. Future refinements of the MELTS will undoubtedly close the gap between predictions and observations and enhance the value of this tool.

The latest version of the model, *pMELTS* runs on UNIX-based computers (including Mac OS X), and is available on World Wide Web at "http://melts.ofm-research.org/index.html"). This web site also has an online *Java* version available.

4.7 REPRISE: THERMODYNAMICS OF ELECTROLYTE SOLUTIONS

We discussed the nature of electrolyte solutions and introduced one approach to dealing with their non-ideality, namely the Debye-Hückel activity coefficients, in Section 3.7. We also noted a number of theoretical weaknesses in the Debye-Hückel approach and that this approach is restricted to fairly dilute solutions (ionic strengths less than 0.1 M). In this section we will return to the problem of electrolyte solutions and examine the causes of non-ideal behavior in high ionic strength solutions in more detail. Before doing so, however, we need to introduce a new variation on our now-familiar thermodynamic parameters, namely mean ionic quantities.

4.7.1 Mean Ionic Quantities

Consider an aqueous NaCl solution. In Chapter 3 we saw that the thermodynamic properties of a salt are related to those of its component ions by:

$$\Psi_{AB} \equiv \nu_A \Psi_A + \nu_B \Psi_B \tag{3.73}$$

So, for example, the chemical potential of NaCl in solution is:

$$\mu_{NaCl} = \mu_{Na^+} + \mu_{Cl^-}$$

which we can express as:

$$\mu_{NaCl} = \mu^o_{Na^+} + \mu^o_{Cl^-} + RT\left(\ln a_{Na^+} + \ln a_{Cl^-}\right) \tag{4.69}$$

or:

$$\mu_{NaCl} = \mu^o_{Na^+} + \mu^o_{Cl^-} + RT\left(\ln m_{Na^+} + \ln m_{Cl^-}\right) + RT\left(\ln \gamma_{Na^+} + \ln \gamma_{Cl^-}\right)$$

Though we can certainly determine the concentrations of Na and Cl in solution, how do we independently determine their activity coefficients? Since we cannot create a pure Na^+ solution or a pure Cl^- one, we cannot say what part of the non-ideality of NaCl solution is due to Na^+ and what part is due to Cl^-. The practical solution then is to assign all non-ideality equally to both ions. This leads to the concept of the *mean ion activity coefficient*:

$$\gamma_\pm = (\gamma_{Na^+}\gamma_{Cl^-})^{1/2} \tag{4.70}$$

Thus the mean activity coefficient of a salt is the geometric mean of the activity coefficients of its component ions. Equation 4.69 then becomes:

$$\mu_{NaCl} = \mu^o_{Na^+} + \mu^o_{Cl^-} + RT\left(\ln m_{Na^+} + \ln m_{Cl^-} + \ln \gamma_\pm^2\right)$$

Equation 4.70 is valid for 1:1 salts (i.e., 1 cation for each anion). A general expression for the mean activity coefficient of a salt of composition $A_{\nu+}B_{\nu-}$ is:

$$\gamma_\pm = (\gamma_+^{\nu^+}\gamma_-^{\nu^-})^{1/\nu} \qquad 4.71$$

where ν is the sum of the component positive and negative ions:

$$\nu = \nu^+ + \nu^- \qquad 4.72$$

Mean activity coefficients have the advantage that they are readily measurable (through electrochemical means or solubility, for example). Given a well-behaved salt, such as KCl, where the relationship $\gamma_- = \gamma_+$ appears to hold, it is then possible to determine single ion activity coefficients. For example, we can obtain γ_{Na^+} in our NaCl solution by first determining γ_{Cl^-} in KCl*:

$$\gamma_{Cl^-} = \gamma_{K^-} = \gamma_{\pm KCl}$$

then determining the mean ion activity coefficient of NaCl experimentally *in a solution of the same ionic strength* and calculating γ_{Na^+} as:

$$\gamma_{Na^+} = \frac{\gamma^2_{\pm NaCl}}{\gamma_{Cl^-}}$$

We can extend the concept of mean ionic quantities to other thermodynamic variables as well. The *mean ionic potential*, $\mu_\pm$, is defined as:

$$\mu_\pm = \frac{\nu^+\mu_+\nu^-\mu^-}{\nu} \qquad 4.73$$

Thus the mean ionic potential is simply the arithmetic mean of the potential of the individual ions weighted by their stoichiometric coefficients. We could also express the mean ionic potential as:

$$\mu_\pm = \mu^o_\pm + \frac{RT\left(\ln a_+^{\nu^+} + \ln a_-^{\nu^-}\right)}{\nu} \qquad 4.74$$

Rearranging once more, we obtain:

$$\mu_\pm = \mu^o_\pm + RT\ln\left(a_+^{\nu^+}a_-^{\nu^-}\right)^{1/\nu} \qquad 4.75$$

Comparing this relationship with equation 4.69, we define a *mean ionic activity* such that:

$$a_\pm = \left(a_+^{\nu^+}a_-^{\nu^-}\right)^{1/\nu} \qquad 4.76$$

Example 4.5: Calculating Single Ion Activity Coefficients from Mean Ionic Activity Coefficients

The measured mean ionic activity coefficient of KCl in a solution of 1.0 m ionic strength is 0.604; that of $CaCl_2$ in a solution of the same ionic strength is 0.449. What is the activity coefficient of Ca^{2+}? Assume $\gamma_{Cl^-} = \gamma_{K^+}$.

Answer: We begin by noting that $\gamma_{Cl^-} = \gamma_{K^+} = \gamma_{\pm KCl}$ and therefore that $\gamma_{Cl^-} = 0.604$. According to equ. 4.71, the mean ion activity coefficient for $CaCl_2$ is related to the single ion activity coefficients as:

$$\gamma_{\pm CaCl_2} = \left(\gamma_{Ca^+}\gamma^2_{Cl^-}\right)^{1/3}$$

Solving this for $\gamma_{Ca^{2+}}$ we have:

$$\gamma_{Ca^+} = \frac{\gamma^3_{\pm CaCl_2}}{\gamma^2_{Cl^-}} = \frac{0.449^3}{0.604^2} = 0.248$$

* The use of KCl as a reference for determining mean ion activity coefficients is based on the observation that K^+ and Cl^- have about the same effective radius and ion mobility and is known as the MacInnes Convention. Like that of Debye-Hückel, however, this approach breaks down at high ionic strength.

We can also define mean ionic molalities such that $a_\pm = \gamma_\pm m_\pm$. Substituting $a_- = \gamma_- m_-$, and $a_+ = \gamma_+ m_+$, we find the *mean ionic molality* is then:

$$m_\pm = \left(m_+^{\nu^+} m_-^{\nu^-}\right)^{1/\nu} \qquad 4.77$$

Mass balance requires that:

$$m^+ = \nu^+ m \quad \text{and} \quad m^- = \nu^- m \qquad 4.78$$

Substituting this into equation 4.77, we see that:

$$m_\pm = m\left(\nu_+^{\nu^+} \nu_-^{\nu^-}\right)^{1/\nu} \qquad 4.79$$

Let's return to our NaCl example. Dissociation is essentially complete and ν^+ and ν^- are unity, so that:

$$m_{Na^+} = m_{NaCl}$$

and

$$m_{Cl^-} = m_{NaCl}$$

Since $\nu = 2$:

$$m_{\pm NaCl} = \sqrt{m_{NaCl}^2} = m_{NaCl}$$

Mean ionic molality is simply equal to molality for a completely dissociated salt consisting of monovalent ions such as NaCl.

The mean ionic activity coefficient, or the *stoichiometric activity coefficient* as it's sometimes referred to, of NaCl would be the square root of the product of the component activity coefficients according to equation 4.76, as would the mean ionic activity. The individual ion activities can be measured in a number of ways. Therefore, the above relationships allow calculation of the mean ionic activity coefficient from measurable quantities.

For strong electrolytes, i.e., salts that completely dissociate, it can also be shown that mean activity coefficient and mean activity of the salt are related to its activity coefficient and activity by:

$$\gamma = \gamma_\pm^\nu \qquad 4.80$$

and

$$a = a_\pm^\nu \qquad 4.81$$

We can modify the Debye-Hückel equations to obtain mean ion activity coefficients as follows:

Debye-Hückel Extended Law:

$$\log_{10}\gamma_\pm = \frac{-Az_+|z_-|\sqrt{I}}{1 + B\mathring{a}\sqrt{I}} \qquad 4.82$$

Limiting Law:

$$\log_{10}\gamma_\pm = -Az_+|z_-|\sqrt{I} \qquad 4.83$$

where å is taken as the sum of the radii of the anion and cation, i.e., $\mathring{a} = \mathring{a}_+ + \mathring{a}_-$.

EXAMPLE 4.6: MEAN IONIC PARAMETERS FOR A FULLY DISSOCIATED ELECTROLYTE

If the molality of a $CaCl_2$ solution is 0.3 M and the activity coefficients of Ca^{2+} and Cl^- are 0.5 and 0.7 respectively, calculate the activity and mean ionic molality of $CaCl_2$ in the solution. Assume that $CaCl_2$ fully dissociates.

Answer: For $CaCl_2$, $\nu^+ = 1$, $\nu^- = 2$, and $\nu = 3$. So we can use equation 4.79 to calculate mean ionic molality:

$$m_{\pm CaCl_2} = m_{CaCl_2}(1^1 2^2)^{1/3} = 4^{1/4} m_{CaCl_2}$$

Substituting 0.3 for m, we find that $m_\pm = 0.4762$ M.

We then use equation 4.71 to calculate the mean ionic activity coefficient:

$$\gamma_\pm = (\gamma_+^{\nu^+}\gamma_-^{\nu^-})^{1/\nu} = (0.5^1 0.7^2)^{1/3} = 0.625$$

The mean ionic activity is then:

$$a_\pm = \gamma_\pm m_\pm = 0.625 \times 0.4762 = 0.298$$

and the activity of $CaCl_2$ is:

$$a_{CaCl_2} = a_\pm^\nu = \gamma_\pm m_\pm = 0.298^3 = 0.0263M$$

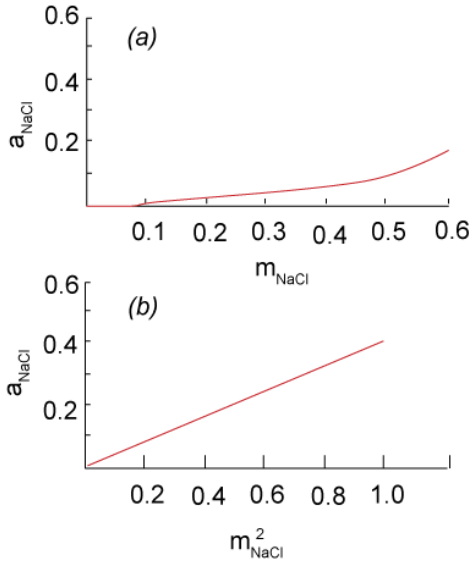

Figure 4.25. (a) Relationship between activity and molality of NaCl in aqueous solution. The activity is very low and the "Henry's Law Slope" is almost 0 at low concentrations. (b) Relationship between activity and the square of molality of NaCl in aqueous solution.

4.7.1.1 Relationship between Activity and Molality of a Salt

Let's consider the relationship between activity and molality of a salt in an electrolyte solution such as a NaCl solution. Figure 4.25a illustrates this relationship. What we immediately notice is that the slope in the Henry's Law region is essentially zero, which is not at all what we expect for Henry's Law behavior.

It can easily be shown that the relationship in Fig. 4.25a is a simple consequence of the dissociation of the NaCl into Na^+ and Cl^- ions. From 3.75 we have:

$$\mu_{NaCl} = \mu_{Na^+_{aq}} + \mu_{Cl^-_{aq}} \qquad 4.84$$

Substituting this into equation 3.46, we obtain:

$$\mu_{NaCl} = \mu^o_{Na^+} + \mu^o_{Cl^-} + RT \ln a_{Na^+} + RT \ln a_{Cl^-}$$

In the reference state of infinitely dilute solution, $m_i = a_i$, so that:

$$\mu_{NaCl} = \mu^o_{Na^+} + \mu^o_{Cl^-} + RT \ln m_{Na^+} + RT \ln m_{Cl^-} \qquad 4.85$$

Furthermore, charge balance requires that:

$$m_{Na^+} = m_{Cl^-} = m_{NaCl} \qquad 4.86$$

Substituting 4.86 into 4.85 and rearranging:

$$\mu_{NaCl} = \mu^o_{Na^+} + \mu^o_{Cl^-} + 2RT \ln m_{NaCl} = \mu^o_{Na^+} + \mu^o_{Cl^-} + RT \ln m^2_{NaCl} \qquad 4.87$$

Comparing this equation with equation 3.46, we see that

$$a_{NaCl} \propto m^2_{NaCl}$$

When we plot activity versus the square of molality, we obtain a linear relationship (Fig. 4.25b).

Generalizing this result for dissociation of a substance into a positive ion A and negative ion B, such as:

$$A_{\nu^+} B_{\nu^-} \cdots \nu^+ A^{\nu^+} + \nu^+ B^{\nu^-}$$

the relationship between activity of a salt and its molality is:

$$\boxed{a_{AB} \propto m^\nu_{AB}} \qquad 4.88$$

For example, ν is 3 for $CaCl_2$, 4 for $FeCl_3$, etc.

Now let's see what happens if we substitute the mean ion activity for activity. Since:

$$a^\nu_\pm = a_{AB}$$

We have: $a^\nu_\pm = m^\nu_{AB}$ or $a_\pm \propto m_{AB}$

This is the relationship that we observed in Figure 4.25, so we see that the mean ionic activity accounts for the effects of dissociation.

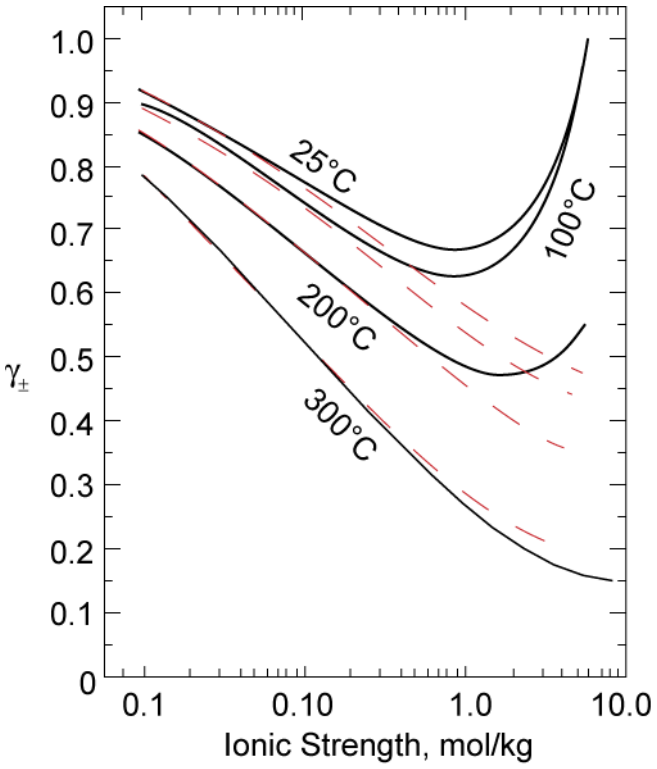

Figure 4.26. Observed mean ion activity coefficient, $\gamma_\pm$, of NaCl as a function of ionic strength and temperature (solid lines; data from Helgeson, 1981) compared with value predicted by the Debye-Hückel Law (dashed red lines, computed as $(\gamma_{Na^+}\gamma_{Cl^-})^{1/2}$).

4.7.2 Activities in High Ionic Strength Solutions

The Debye-Hückel equation becomes inaccurate at ionic strengths above about 0.1 m.

This is illustrated in Figure 4.26, which shows the experimentally determined mean ion activity coefficient for NaCl as a function of ionic strength and temperature. At low temperatures, the activity begins to increase about ionic strengths of 1 m, whereas Debye-Hückel predicts continual decrease. The activities of many electrolytes eventually exceed 1 at high concentrations. The difference between the observed activity coefficients and those predicted by the Debye-Hückel equation are due to the effects of ion association and solvation. Debye and Hückel explicitly assumed complete dissociation, i.e., no ion associations, and while their treatment included in a general way the dielectric properties of water, it neglected the effects of solvation. As we noted in Chapter 3, the effects of both ion association and solvation become increasingly important with increasing ionic strength. It should be no surprise then that the Debye-Hückel treatment breaks down at high ionic strength. Here we will consider these effects in greater detail.

4.7.2.1 Correction for the Concentration of Water

At low and moderate ionic strength, we can assume that the mole fraction of water in solution is 1. For example in seawater, with an ionic strength of 0.7, the mole fraction of water about 0.99. Generally, activity coefficients and equilibrium constants are not known within 1%, so the error introduced by this assumption is still small compared to other errors. In higher ionic strengths, however, this assumption is increasingly invalid (for example, at a molality of 3, the mole fraction of water has decreased below 0.95), and this must be taken into account. A convenient way to do this is to incorporate it into the activity coefficient. The corrected activity coefficient is:

$$\gamma_{corr} = \frac{\gamma}{\left(1 + 0.018 \sum_i m_i\right)} \qquad 4.89$$

4.7.2.2 Effects of Solvation

Water molecules bound to ions in solvation shells have lost their independent translational motion and move with the ion as a single entity. These water molecules are effectively unavailable for reaction, hence solvation has the effect of reducing the activity of water, which increases the apparent concentration, or activity, of the solutes. In addition to solvation, i.e., the direct association of some water molecules with the ion, the charge of the ion causes collapse of the water structure beyond the solvation shell.

For a solution consisting of a single salt, Robinson and Stokes (1959) proposed the contribution of solvation to the mean ion activity coefficient could be expressed as:

$$\log \gamma_{\pm}^{solv} = -\frac{h}{\nu} \log a_w - \log(1 - 0.018 h m) \qquad 4.90$$

where $\gamma_{\pm}^{solv}$ is the solvation contribution to the mean ion activity coefficient, h is the number of moles of water molecules bound to each mole of salt, a_w is the activity of water, m is the concentration of the salt in solution, and ν is a defined in equation 4.72 (i.e., total moles of ions produced upon dissolution of a mole of salt). Table 4.3 listed estimated values for the solvation number, i.e., number of water molecules in the solvation shell of each ion. From these, the value of h for equ. 4.90 can be calculated. The activity of water can be adequately estimated as:

$$a_w = 1 - 0.04m$$

Figure 4.27 illustrates the effect of solvation on the activity coefficient. As may be seen, solvation sub-

Table 4.03. Ion Solvation Numbers

Species	h	Species	h
Li^+2.3	OH^-	7.6	
Na^+	3.3	F^-	6.7
K^+	2.3	Cl^-	2.7
Rb^+	2.3	Br-	1.7
Mg^{2+}	8.9	CO_3^{2-}	14.4
Ca^{2+}	8.9	SO_4^{2-}	10.4
Cd^{2+}	6.3		
Ba^{2+}	9.2		

stantially affects the activity coefficient at ionic strengths above about 0.5 m.

4.7.2.2 Effects of Ion Association

An ion pair can be considered to have formed when ions approach closer than some critical distance, r_c, where the electrostatic energy, which tends to bind them, exceeds twice the thermal energy, which tends to move them apart. When this happens, the ions are electrostatically bound and their motions are linked. They are said to form an ion pair. The thermal energy of an ion is kT and electrostatic interaction energy is:

$$U_{electro.} = \frac{q_1 q_2}{4\pi\varepsilon r} \qquad 4.91$$

The ratio of these two energies when the distance is less than the critical one is then:

$$\frac{U_{electro}}{U_{therm}} = \frac{z_1 z_2 e^2}{4\pi\varepsilon_0 \varepsilon_r r T} \qquad 4.92$$

We can use this equation to solve for the critical distance r_c:

$$r_c = \frac{z_1 z_2 e^2}{8\pi\varepsilon_0 \varepsilon_r T} \qquad 4.93$$

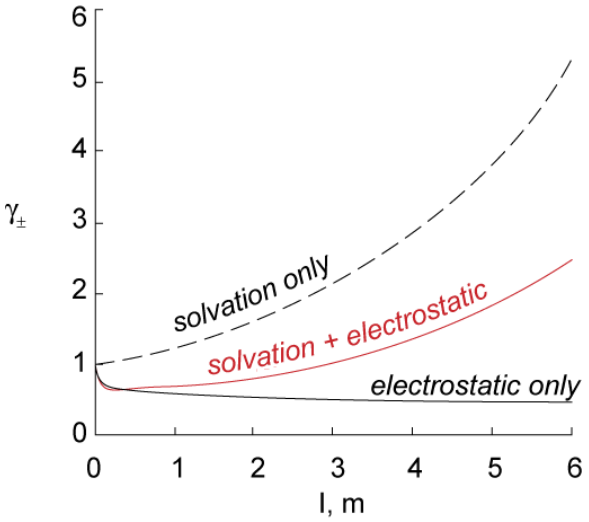

Figure 4.27. Comparison of the electrostatic contribution to the mean ion activity coefficient of NaCl (calculated by the Debye-Hückel Extended Law), the solvation contribution (calculated from equation 4.92 assuming $h = 4$) and the sum of the two.

For two singly charged ions, the critical distance is 3.57 Å. In a 1 molar solution, the average separation between ions is about 12 Å, so even in such a relatively concentrated solution, ion pairs will not form between singly charged ions. Indeed, the critical distance is smaller than the combined Debye-Hückel radii of all pairs of singly charged ions. Thus we do not expect ion associations to form from pairs of singly charged ions under most circumstances. In contrast, the critical distance for ion association between a singly and a doubly charged ion is 70 Å, considerably greater than the sum of their Debye-Hückel radii. It also exceeds the average separation of ions in a 0.01 m solution (about 55 Å), so that even in dilution solutions, we would expect significant ion pair formation for multiply charged ions.

As we saw earlier, all ions in solution are surrounded by a solvation shell of water molecules. This solvation shell may or may not be disrupted when ion pair formation occurs (Fig. 4.28). If it is not disrupted, and the two solvation shells remain intact, an *outer sphere ion pair* (also called an outer sphere complex) is said to have formed. If water molecules are excluded from the space between the ions, an *inner sphere ion pair* (or complex) is said to have formed.

For some purposes, ion pairs can be treated as distinct species having charge equal to the algebraic sum of the charge of the ions involved. These can be included, for example, in calculation of ionic strength to obtain a somewhat more accurate estimate of activities. On the other hand, ion pairs, including neutral ones, can be highly dipolar and may behave as charge-separated ions.

Ion associations affect activities in two ways. First, associated ions are less likely to participate in reactions, thus reducing the activity of the ions involved. Second, ion association reduces the ionic strength of the solution, and hence reduces the extent of electrostatic interactions among ions. This has the effect of increasing activity. To understand the first effect, consider the case where a certain fraction of the free ions re-associates to form ion pairs, e.g.:

$$\nu^+ A^{z+} + \nu^- B^{z-} \rightleftarrows (A_{\nu^+} B_{\nu^-})^0_{aq}$$

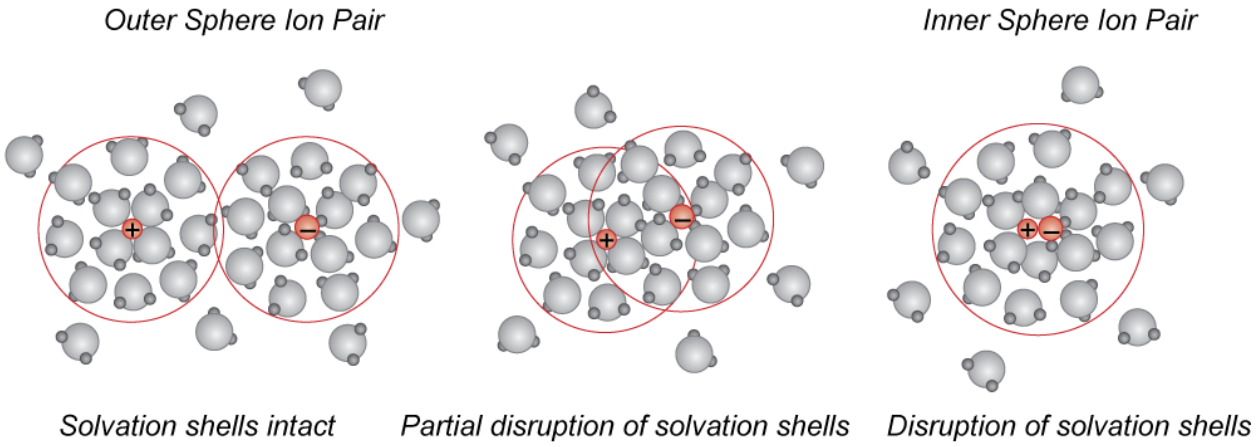

Figure 4.28. In formation of ion pairs, the solvation shells may remain intact or be partially or totally disrupted. The former results in an outer sphere ion pair, the latter results in an inner sphere ion pair.

where the superscript 0 indicates neutrality and the subscript *aq* a dissolved aqueous species. A salt that only partially dissociates in solution is called a weak electrolyte. Let α be the fraction of the ions that associate to form ion pairs or complexes. The associate of this fraction of ions as ion pairs will be thermodynamically equivalent to that fraction of the substance not dissociating to begin with. The fraction of free ions is then 1 – α. Equation 4.78 becomes:

$$m^+ = (1-\alpha)\nu^+ m \quad \text{and} \quad m^- = (1-\alpha)\nu^- m \tag{4.94}$$

where m is the molality of the solute. We can rewrite equation 4.76 as:

$$a_\pm = \left[(\gamma_+ m_+)^{\nu^+} (\gamma_- m_-)^{\nu^-} \right]^{1/\nu} \tag{4.95}$$

Substituting 4.94 into 4.95 and rearranging, we obtain:

$$a_\pm = \left(\gamma_+^{\nu^+}\gamma_-^{\nu^-}\right)^{1/\nu} \left\{ \left[(1-\alpha)\nu^+ m\right]^{\nu^+} \left[(1-\alpha)\nu^- m\right]^{\nu^-} \right\}^{1/\nu}$$

A little more rearranging and we have:

$$a_\pm = \left(\gamma_+^{\nu^+}\gamma_-^{\nu^-}\right)^{1/\nu} \left\{ \left[(1-\alpha)m\right]^{(\nu^+ + \nu^-)} \left(\nu^+\right)^{\nu^+} \left(\nu^-\right)^{\nu^-} \right\}^{1/\nu}$$

Finally, since $\nu = \nu^+ + \nu^-$, we obtain:

$$a_\pm = \left(\gamma_+^{\nu^+}\gamma_-^{\nu^-}\right)^{1/\nu} (1-\alpha) m \left\{ \left(\nu^+\right)^{\nu^+} \left(\nu^-\right)^{\nu^-} \right\}^{1/\nu} \tag{4.96}$$

We can recognize the last term as $m_\pm$. Since $a_\pm = \gamma_\pm m_\pm$, we see that the mean ionic activity coefficient will be

$$\gamma_\pm = (1-\alpha)\left(\gamma_+^{\nu^+}\gamma_-^{\nu^-}\right)^{1/\nu} \tag{4.97}$$

for an incompletely dissociated electrolyte. Thus the mean ion activity coefficients are reduced by a factor of 1 – α. Provided we have appropriate stability constants for the ion pairs or complexes, α can be calculated and an appropriate correction applied.

Now consider a $CaSO_4$ solution of which some fraction of the Ca^{2+} and SO_4^{2-} ions, α, associate to form $CaSO_4^\circ$. The ionic strength of the this solution would be

$$I = \frac{(1-\alpha)}{2}\left(4m_{Ca^{2+}} + 4m_{SO_4^{2-}}\right)$$

Thus the ionic strength is reduced by a factor of 1 - α as well.

Ion pairs and complexes need not be neutral species ($AlCl^{2+}$, for example). When they are not, they will contribute to ionic strength. A general expression for ionic strength taking account of ion associations must include charged ion pairs and complexes:

$$I = \frac{1}{2}\left[\sum_i (1-\alpha) m_i z_i^2 + \sum_n c_n z_n^2\right] \quad 4.98$$

where α_i is the fraction of each ion involved in ion associations, and c_n is the concentration of each ion pair or complex and z_n is its charge. We could use this result directly in the Debye-Hückel equation to make an improved estimate of ionic strength, and hence of the single ion activity coefficient.

Figure 4.29 illustrates the effect of ion pair formation for a hypothetical $CaCl_2$ solution in which some fraction of the ions combine to form ion pairs. The fraction of Ca^{2+} ions forming $CaCl^-$ was assumed to increase linearly with ionic strength up to the maximum value shown.

EXAMPLE 4.7. ACTIVITY COEFFICIENTS IN A BRINE

The following concentrations were measured in a shield brine from Sudbury, Canada at 22° C. Calc ulate the activity coefficients of th ese species using the Truesdell-Jones equation.

Species	Conc g/kg
Na	18.9
K	0.43
Ca	63.8
Mg	0.078
SO_4	0.223
HCO_3	0.042
Cl	162.7

Answer: Our first task is to convert g/kg to molal concentrations. We do this by dividing by molecular weight. Next, we need to calculate ionic strength (equation 3.75) which we find to be 5.9 m. Calculation of activity coefficients is then straightforward using the parameters in Tables 3.2 and 4.6. Finally, we apply a correction for the decreased concentration of water (equation 4.89). Our final spreadsheet is shown below.

	‰	m	z	å_TJ	b_TJ	log (gamma)	ganma	gamma corr
Na	18.9	0.822	1	5	0.165	0.728	5.341	4.741
K	0.43	0.017	1	3.5	0.015	-0.238	0.579	0.514
Ca	63.8	1.595	2	5	0.165	-0.017	0.963	0.855
Mg	0.078	0.003	2	5.5	0.2	0.264	1.836	1.630
SO4	0.223	0.002	2	5	-0.04	-1.229	0.059	0.052
HCO3	0.058	0.001	1	5.4	0	-0.233	0.585	0.519
Cl	162.7	4.590	1	3.5	0.015	-0.238	0.579	0.514
	m	7.030	A	0.5092				
	I	5.913	B	0.3283				

If the formation of ion pairs depends on the ratio of thermal to electrostatic energy, we might expect that ion pair formation will decrease with temperature. However, the relative permittivity of water decreases with temperature, allowing increased electrostatic interaction between ions, and this effect dominates over the increased thermal energy of ions. As a result, the extent of ion association increases with temperature. Increasing pressure, on the other hand, favors dissociation of ions.

4.7.2.2 Alternative Expressions for Activity Coefficients

There have been a number of attempts to develop working equations that account for all the effects on activity coefficients at high ionic strength. Many of these are ultimately based on the specific ion interaction theory of Brønsted (1922). Brønsted proposed an equation of the form:

$$\log \gamma_i = \alpha m^{1/2} + \beta_i m \qquad 4.99$$

where α is a constant that is independent of the solute ions and β is the "specific ion interaction parameter" and is different for each ionic species. Guggenheim (1935) replaced the first term on the right with a simplified form of the Debye-Hückel equation and the second term with the summation of ion-ion interaction parameters:

$$\log \gamma_i = \frac{-z_i^2 A\sqrt{I}}{1+\sqrt{I}} + 2\sum_k \beta_{i,k} m_k \qquad 4.100$$

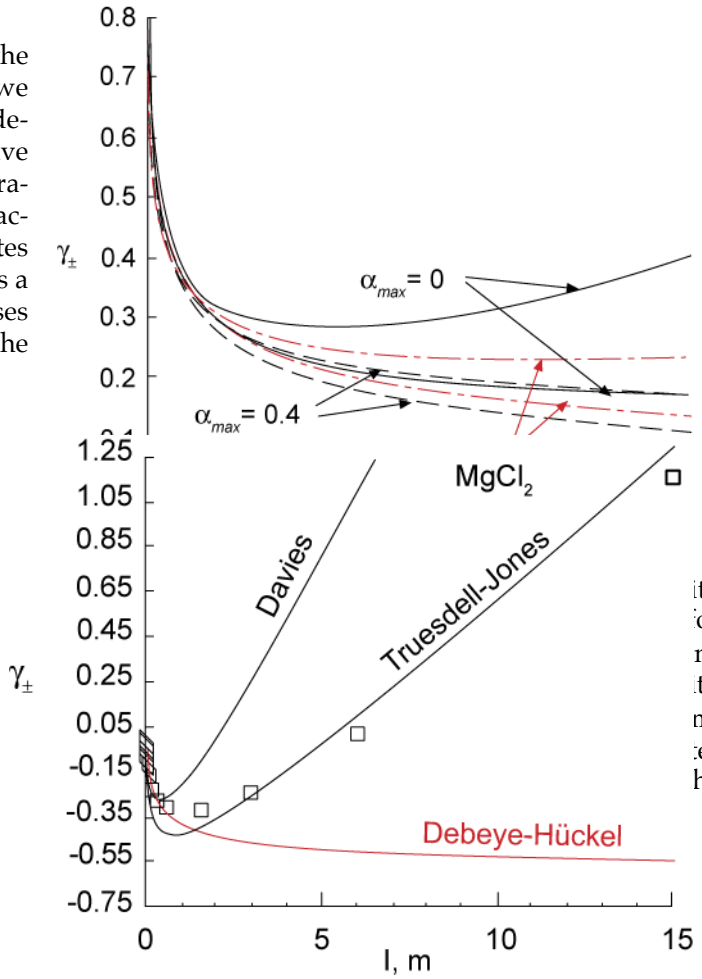

Figure 4.30. Measured mean ionic activity coefficients in $MgCl_2$ solution as a function of ionic strength compared with values calculated from the Debye-Hückel, Davies and Truesdell-Jones equations.

where β_{ik} is parameter describing the interactions between ions *i* and *k*. For natural waters with many species, the Guggenheim equation becomes complex. Also starting from Debye-Hückel, Truesdell and Jones (1974) proposed the following simpler equation:

$$\log \gamma_i = \frac{-z_i^2 A\sqrt{I}}{1+B\mathring{a}_i\sqrt{I}} + b_i I \quad \log \gamma_i = \frac{-z_i^2 A\sqrt{I}}{1+B\mathring{a}_i\sqrt{I}} + b_i I \qquad 4.101$$

The first term on the right is identical in form to Debye-Hückel; the second term is similar to the Brønsted specific ion interaction term. Truesdell and Jones determined parameters å and b empirically. Table 4.5 lists these parameters for some common ions. Figure 4.30 compares mean activity coefficient of calculated with the Debye-Hückel, Davies, and Truesdell-Jones equations with the actual measured values. The Truesdell-Jones equations fit these observations very well. This is not always the case, however. The fit for Na_2CO_3, for example is little better than for Debye-Hückel.

Other equations include those developed by Pitzer (1979) and the National Bureau of Standards. While these equations are generally more accurate than the above, their complexity places them beyond the scope of this book. The interested reader is referred to any of several texts on geochemical ther-

modynamics that treat them (Nordstrom and Munoz, 1986; Fletcher, 1993; Anderson and Crerar, 1993) as well as the original literature.

References and Suggestions For Further Reading

Anderson, G. M. and D. A. Crerar. 1993. *Thermodynamics in Geochemistry*. New York: Oxford Univ. Press.

Bohlen, S. R., W. A. Dollase and V. J. Wall. 1986. Calibration and application of spinel equilibria in the system FeO-Al_2O_3-SiO_2. *J. Petrol.* 27: 1143-1156.

Bohlen, S. R. and D. H. Lindsley, 1987. Thermometry and barometry of igneous and metamorphic rocks. *Ann. Rev. Earth Planet. Sci.* 15:397-420.

Bohlen, S. R., V. J. Wall and A. L. Boettcher. 1983. Experimental investigations and geologica applications of equilibria in the system FeO-TiO_2-Al_2O_3-SiO_2-H_2O. *Am. Mineral.* 68: 1049-1058.

Bottinga, Y. and D. Weill. 1972. The viscosity of magmatic silicate liquids: a model for calculation. *Am. J. Sci.* 272: 438-475.

Boyd, F.R. 1973. A pyroxene geotherm. *Geochim. Cosmochim. Acta,* 37, 2533-2546.

Bradley, R. S. 1962. Thermodynamic calcuations on phase equilibria involving fused salts. Part II. Solid solutions and applications to the olivines. *Am. J. Sci.*, 260, 550-554.

Brønsted, J. N. 1922. Studies on solubility, IV. The principle of specific interaction of ions. *J. Am. Chem. Soc.* 44: 877-898.

Buddington, A. F. and D. H. Lindsley. 1964. Iron-titanium oxide minerals and synthetic equivalents, *J. Petrol.* 5: 310-357.

Carmichael, I. S. E. and H. P. Eugster (eds). 1987. *Thermodynamic Modeling of Geological Materials: Minerals, Fluids and Melts (Reviews in Mineralogy, vol 17)*. Washington: Mineral. Soc. Am.

Essene, E. 1982. Geologic thermometry and barometry. **In** *Characterization of metamorphism through mineral equilibria, Reviews in Mineralogy Vol. 10*, J. M. Ferry. ed., pp. 153-206. Washington: Mineral. Soc. Am.

Essene, E. 1989. The current status of thermobarometry in metamorphic rocks. **In** *The Evolution of Metamorphic Belts, Vol.* J. S. Daly, R. A. Cliff and B. W. D. Yardley. ed., pp. 1-44. London: Blackwell Sci. Pub.

Ferry, J. M. and F. S. Spear. 1978. Experimental calibration of the partitioning of Fe and Mg between biotite and garnet. *Contrib. Mineral. Petrol.* 25: 871-893.

Fletcher, P. 1993. *Chemical Thermodynamics for Earth Scientists*, Essex: Logman Scientific and Technical.

Garrels, R. M., and Christ, C. L. 1965. *Solutions, Minerals, and Equilibria*. New York: Harper and Row.

Gasparik, T. 1984a. Two-pyroxene thermobarometry with new experimental data in the system CaO-MgO-Al_2O_3-SiO_2. *Contrib. Mineral. Petrol.* 87: 87-97.

Gasparik, T. 1984b. Experimental study of subsolidus phase relations and mixing properties of pyroxene and plagioclase in the system CaO-Al_2O_3-SiO_2. *Geochim. Cosmochim. Acta*. 48: 2537-2446.

Ghent, E. D. 1976. Plagioclase-garnet-Al_2O_5-quartz: a potential geobarometer-geothermometer. *Am. Mineral.* 61: 710-714.

Ghiorso, M. S. 1987. Modelling magmatic systems: Thermodynamic relations. in *Thermodynamic Modelling of Geological Materials: Minerals, Fluids, and Melts*. eds. I. S. E. Carmichael and H. P. Eugster. 443-465. Washington: Mineral. Soc. Am.

Ghiorso, M. S. and I. S. E. Carmichael. 1985. Chemical mass transfer in magmatic processes: II. Applications in equilibrium crystallization, fractionation crystallization, and assimilation, *Contrib. Mineral. Petrol.* 90: 121-141.

Ghiorso, M. S., I. S. E. Carmichael, M. L. Rivers and R. O. Sack. 1983. The Gibbs free energy of mixing of natural silicate liquids; an expanded regular solution approximation for the calculation of magmatic intensive variables. *Contrib. Mineral. Petrol.* 84: 107-145.

Ghiorso, M. S., M. M. Hirshmann and R. O. Sack. 1994. New software models thermodynamics of magmatic systems. *EOS*. 75: 571-576.

Ghiorso, M. S., M. M. Hirschmann, P. W. Reiners and V. C. Kress, 2002. The pMELTS: a revision of MELTS for improved calculation of phase relations and major element partitioning related to partial melting of the mantle to 3 GPa, *Geochem. Geophys. Geosyst.*, 3:2001GC000217.

Ghiorso, M. S. and R. O. Sack. 1995. Chemical mass transfer in magmatic processes IV. A revised and internally consistent thermodynamic model for the interpolation and extrapolation of liquid-solid equilibria in magmatic systems at elevated temperatures and pressures. *Contrib. Mineral. Petrol.* 119: 197-212.

Goldsmith, J. R. and R. C. Newton. 1969. P-T-X relations in the system $CaCO_3$-$MgCO_3$ at high temperatures and pressures. *Am. J. Sci.* 267A: 160-190.

Grover, J., 1977. Chemical mixing in multicomponent solutions: An introduction to the use of margules and other thermodynamic excess functions to represent non-ideal behavior, in *Thermodynamics in Geology*. ed. D. G. Fraser. 67-97. Dordrecht: D. Reidel.

Guggenheim. 1935. The specific thermodynamic properties of aqueous solutions of strong electrolytes. *Phil. Mag.* 19: 588.

Helgeson, H. C. 1969. Thermodynamics of hydrothermal systems at elevated temperatures and pressures. *Am. J. Sci.* 267: 729-804.

Helgeson, H. C. and D. H. Kirkham. 1974. Theoretical prediction of the thermodynamic behavior of aqueous electrolytes at high pressures and temperatures, Debye-Hückel parameters for activity coefficients and relative partial molar quantities. *Am J. Sci.* 274: 1199-1261.

Helgeson, H. C., Kirkham, D. H., and G. C. Flowers. 1981. Theoretical predicitons of the thermodynmaic behavior of electrolytes at high pressures and temperatures: IV. Calculation of activity coefficients, osmotic coefficients, and apparent molar and standard and relative partial molar properties to 600°C and 5 kbar. *Am. J. Sci.* 281: 1249-1316.

Holdaway, M. J. 1971. Stability of andalusite and the aluminum silicate phase diagram. *Am. J. Sci.* 271: 91-131.

Holland, T. J. B., A. Navrotsky, and R. C. Newton, 1979. Thermodynamic parameters of $CaMgSi_2O_6$ – $Mg_2Si_2O_6$ pyroxenes based on regular solution and cooperative disordering models. *Contrib. Mineral. Petrol.* 69: 337-344.

Johannes, W. and D. Puhan. 1971. The calcite-aragonite equilibrium reinvestigated. *Contrib. Mineral. Petrol.* 31: 28-38.

Koziol, A. M. and R. C. Newton. 1988. Redetermineation of the garnet breakdown reaction and improvement of the plagioclase-garnet-Al_2O_5-quartz geobarometer. *Am. Mineral.* 73: 216-223.

Navrotsky, A. 1994. *Physics and Chemistry of Earth Materials*. Cambridge: Cambridge University Press.

Nicholls, J. and J. K. Russell. 1990. *Modern Methods in Igneous Petrology, Reviews in Mineralology, vol. 24,* Washington: Min. Soc. Am.

Nielsen, R. L. and M. A. Dungan. 1983. Low pressure mineral-melt equilibria in natural anhydrous mafic systems, *Contrib. Mineral. Petrol.*, 84: 310-326.

Nordstrom, D. K. and J. L. Munoz, 1986. *Geochemical Thermodynamics*, Palo Alto: Blackwell Scientific Publ.

Pitzer, K. S. 1979. Theory: ion interaction approach. in *Activity Coefficients in Electolytes,* ed. R. M. Pytkowicz. 157-208. Boca Raton: CRC Press.

Powell, R. and T. J. B. Holland, On thermobarometry, Journal of Metamorphic Geology, 26: 155-179, doi: 10.1111/j.1525-1314.2007.00756.x, 2008.

Rankenburg, K., J. C. Lassiter and G. Brey, 2004. Origin of megacrysts in volcanic rocks of the Cameroon volcanic chain - constraints on magma genesis and crustal contamination, *Contr. Mineral. and Petrol.*, 147:129-144.

Robinson, R. A. and R. H. Stokes. 1959. *Electrolyte Solutions*. London: Butterworths.

Roeder, P.L. and R.F. Emslie. 1970. Olivine-liquid equilibrium. *Contrib. Mineral. Petrol.* 29: 275-289.

Spencer, K. and D. H. Lindsley. 1981. A solution model for coexisting iron-titanium oxides. *Am. Mineral.* 66: 1189-1201.

Stolper, E. and H. Y. McSween. 1979. Petrology and origin of the shergottite meteorites. *Geochem. Cosmochim. Acta*. 43: 1475-1498.

Thompson, J. B. 1967. Thermodynamic properties of simple solutions, in *Researches in Geochemistry, vol. 2*, ed. P. H. Abelson. New York: Wiley and Sons.

Thompson, J. B. and D. R. Waldbaum, 1969. Mixing properties of sanidine crystalline solutions: III. Calculations based on two-phase data. *Am. Mineral.* 54: 811–838.

Truesdell, A. H. and B. F. Jones. 1974. WATEQ, a computer program for calculating chemical equilibria in natural waters. *J. Res. U. S. Geol. Surv.* 2: 233-248.

Wood, B. J., 1987. Thermodynamics of multicomponent systems containing several solutions, in *Thermodynamic Modeling of Geological Materials: Minerals, Fluids and Melts*, eds. I. S. E. Carmichael and H. P. Eugster. 71-96. Washington: Mineral. Soc. Am.

Wood, B.J. and S. Banno. 1973. Garnet-orthopyroxene and orthopyroxene-clinopyroxene relationships in simple and complex systems. *Contrib. Mineral. Petrol.* 42:109-124.

ϕ	$\bar{V}$ (cm^3)	S (J/K-mol)
kyanite	44.09	242.30
andalusite	51.53	251.37
sillimanite	49.90	253.05

Problems

1. Kyanite, andalusite, and sillimanite (all polymorphs of Al_2SiO_5) are all in equilibrium at 500°C and 376 MPa. Use this information and the adjacent table to construct an approximate temperature-pressure phase diagram for the system kyanite-sillimanite-andalusite. Assume ΔV and ΔS are independent of temperature and pressure. Label each field with the phase present.

2. Show that: $\overline{G}_{excess} = (W_{G_1} X_2 + W_{G_2} X_1) X_1 X_2$ may be written as a 4 term power expansion, i.e.:

$$\overline{G}_{ex} = A + BX_2 + CX_2^2 + DX_2^3$$

3. Construct G-bar–X diagrams for a regular solution with W= 12 kJ (W is the interaction parameter in a non-ideal solution) at 100° temperature intervals from 200 to 700° C. Sketch the corresponding phase diagram.

4. Interaction parameters for the enstatite-diopside solid solution have been determined as follows: $W_{H\text{-}En}$ = 34.0 kJ/mol, $W_{H\text{-}Di}$ = 24.74 kJ/mol (assume W_V and W_S are 0).

a.) Use the asymmetric solution model to calculate ΔG_{real} as a function of X_2 (let diopside be component 2) curves for this system at 100 K temperature from 1000 K to 1500 K. Label your curves.

b.) What is the maximum mole fraction of diopside that can dissolve in enstatite in this temperature range:?

c.) Sketch the corresponding T-X phase diagram.

5. Sketch G-bar–X diagrams for 1600° C, 1500° C, 1300° C, and 1250° C for the system Diopside-Anorthite (Figure 4.8). Draw tangents connecting the equilibrium liquids and solids.

6. Suppose you conduct a 1 atm melting experiment on a plagioclase crystal. Predict the mole fractions of anorthite in the liquid and solid phases at a temperature of 1425° C. Assume both the liquid and solid behave as ideal solutions. Albite melts at 1118° C, anorthite at 1553°C. ΔH_m for albite is 54.84 kJ/mol; ΔH_m for anorthite is 123.1 kJ/mol.

7. Given the following 2 analyses of basaltic glass and coexisting olivine phenocrysts, determine the K_D for the MgO⇄FeO exchange reaction, and calculate the temperatures at which the olivine crystallized using both MgO and FeO. Assume Fe_2O_3 to be 10 mole% of total iron (the analysis below includes only

the total iron, calculated as FeO; you need to calculate from this the amount of FeO by subtracting an appropriate amount to be assigned as Fe_2O_3). Note that the mole % Fo in olivine is equivalent to the mole % Mg or MgO. (*HINT: you will need to calculate the mole fraction of MgO and FeO in the liquid*).

Glass (liquid) composition:

Sample	TR3D-1 (wt % oxide)	DS-D8A (wt % oxide)
SiO_2	50.32	49.83
Al_3O_2	14.05	14.09
ΣFe as FeO	11.49	11.42
MgO	7.27	7.74
CaO	11.49	10.96
Na_2O	2.3	2.38
K_2O	0.10	0.13
MnO	0.17	0.20
TiO_2	1.46	1.55
olivine		
Mole % Fo (=mole % Mg)	79	81

8. Determine the temperature and oxygen fugacity of equilibration for the following set of coexisting iron-titanium oxides in lavas from the Azores:

	titanomagnetite s.s. phase mole percent magnetite	ilmenite s.s. phase mole percent hematite
G-4 groundmass	29.0	10.3
SJ-8 phenocrysts	41.9	13.0
SM-28 microphenocrysts	54.5	7.0
T-8 groundmass	33.7	8.1
F-29 microphenocrysts	36.2	6.0

Make a plot of f_{O2} vs. temperature using your results and compare with Fig. 3.21. What buffer do the data fall near?

9. Starting from equations 4.54, 4.56 and 4.18, use the fundamental relationships between free energy, entropy, enthalpy, and the equilibrium constant to derive the temperature dependence of the titanomagnetite–ilmenite exchange (equation 4.57).

10. Average Mid-Ocean Ridge Basalt (MORB) has the composition in the table to the right. Use the "web applet" version of MELTS (http://melts.ofm-research.org/index.html) to answer the following question.

a) At a pressure of 500 bars and f_{O2} of QFM -1, what is the liquidus temperature of this magma?

b) If this magma cools and undergoes fractional crystallization of solid phases to a temperature of 1100°C, what would be the composition of the remaining magma? What fraction of liquid would remain?

Oxide	Weight Percent
SiO_2	50.37
TiO_2	1.44
Al_2O_3	15.38
Fe_2O_3	1.10
FeO	8.94
MnO	1.10
MgO	7.92
CaO	11.51
Na_2O	2.70
K_2O	0.18
P_2O_5	0.15
H_2O	0.15

c) If instead the oxygen fugacity were QFM +1, what would be the composition of the remaining magma at 1100°C? How much liquid would remain?

11. In a melt having a composition, in wt %, of:

SiO_2	58.12%	TiO_2	0.92%		
Al_2O_3	16.47%	Fe_2O_3	1.82%		
MgO	5.62%	FeO	9.94%	CaO	7.11%

Use the Ghiorso regular solution model and the interaction parameters in Table 4.3 to:

a.) calculate the $\bar{G}_{ex}$ and $\Delta\bar{G}_{mixing}$ for this composition at 1300°C.

b.) calculate the activity of Si_4O_8 at this temperature.

12. An analysis of an oil field brine from Mississippi with a temperature of 150° C is shown to the right. Calculate the *activities* of these species at that temperature using the Truesdell-Jones equation.

Problem 12

Species	Conc g/kg
Na^+	63.00
K^+	6.15
Mg^{2+}	2.77
Ca^{2+}	44.6
Cl^-	200.4
SO_4^{2-}	0.13
HCO_3^-	0.03

13. Show that for a strong electrolyte, i.e., one in which dissociation is complete and:

$$m_- = \nu_- m \quad \text{and} \quad m_+ = \nu_+ m$$

where m is the molality of the solute component $A_\nu + B_\nu -$, that:

$$m_\pm = m(\nu_+^{\nu_+}\nu_-^{\nu_-})^{1/\nu}$$

where $\nu = \nu_+ + \nu_-$.

14. Mean ionic activity coefficients were measured for the following solutions at an ionic strength of 3: $\gamma_{KCl} = 0.569$, $\gamma_{NaCl} = 0.734$, $\gamma_{Na_2CO_3} = 0.229$. Assuming $\gamma_{Cl^-} = \gamma_{K^-} = \gamma_{\pm KCl}$, what is the activity coefficient of CO_3^{2-}?

15. Calculate the electrostatic and solvation contributions to the mean ionic activity coefficient of $MgCl_2$ at concentrations of 0.0033, 0.01, 0.033, 0.05, 0.1, 0.33, 0.5, and 1 using the Debye-Hückel equation and Robinson and Stokes (equ. 4.92) equ. respectively. Plot results, as well as $\gamma_{elect+solv} = \gamma_{elect}{}^*\gamma_{solv}$ as a function of ionic strength.

16. Calculate the mean ionic activity coefficient for $NaCO_3$ using the Debye-Hückel and Truesdell-Jones equations and compare your results with the observed values to the right. Overall, which fits the data better?

I, m	$\gamma_\pm$ observed
0.001	
0.003	0.887
0.006	0.847
0.01	
0.015	0.78
0.03	0.716
0.06	0.644
0.1	
0.15	0.541
0.3	0.462
0.6	0.385
1	
1.5	0.292
3	0.229
6	0.182